






REVIEW ARTICLE | MARCH 03 2025

# Bulk nonlinear metamaterials for generation of quantum light

Special Collection: [Quantum Metamaterials](#)

O. Yesharim  ; I. Hurvitz  ; J. Foley-Comer  ; A. Arie  

 Check for updates

*Appl. Phys. Rev.* 12, 011323 (2025)

<https://doi.org/10.1063/5.0216714>



View Online



Export Citation

## Articles You May Be Interested In

Transforming underground to surface mining operation – A geotechnical perspective from case study

*AIP Conference Proceedings* (November 2021)

Monthly prediction of rainfall in nickel mine area with artificial neural network

*AIP Conference Proceedings* (November 2021)

Estimation of Karts groundwater based on geophysical methods in the Monggol Village, Saptosari District, Gunungkidul Regency

*AIP Conference Proceedings* (November 2021)



## Special Topics Open for Submissions

[Learn More](#)

# Bulk nonlinear metamaterials for generation of quantum light

Cite as: Appl. Phys. Rev. **12**, 011323 (2025); doi: [10.1063/5.0216714](https://doi.org/10.1063/5.0216714)

Submitted: 30 April 2024 · Accepted: 27 January 2025 ·

Published Online: 3 March 2025



View Online



Export Citation



CrossMark

O. Yesharim, I. Hurvitz, J. Foley-Comer, and A. Arie<sup>a)</sup>

## AFFILIATIONS

School of Electrical Engineering, Fleischman Faculty of Engineering, Tel Aviv University, Tel Aviv 69978, Israel

Note: This paper is part of the APR Special Topic on Quantum Metamaterials.

<sup>a)</sup> Author to whom correspondence should be addressed: [ady@tauex.tau.ac.il](mailto:ady@tauex.tau.ac.il)

## ABSTRACT

Quantum states of light, such as fixed photon number (Fock) states, entangled states, and squeezed states, offer important advantages with respect to classical states of light, such as coherent states and thermal states, in different areas: they enable secure communication and distribution of encryption keys, enable realization of sensors with higher sensitivity and resolution, and are considered candidates for quantum computing and simulation applications. To accommodate these applications, suitable methods for generating the quantum states are needed. Today, the quantum states are often produced by a spontaneous nonlinear process in a standard nonlinear material, followed by a series of optical elements necessary for encoding the desired state on the generated photons. In this review, we consider an alternative approach of structuring the nonlinearity of the crystal so that the desired quantum state will be generated directly at the crystal, without the need for additional elements. Our main focus here is on bulk crystals having structured second-order nonlinearity. The rising interest in these nonlinear metamaterials is fueled by advancements in the ability to efficiently simulate and design spontaneous parametric downconversion (SPDC) processes, as well as by new capabilities of structuring the nonlinearity of ferroelectric crystals, either by electric field poling or by laser-induced writing. As a result, nonlinear metamaterials were recently used to directly shape the spatial and spectral correlations of quantum light that is generated in SPDC. The paper covers the theoretical background and the design and fabrication methods of bulk nonlinear metamaterials for generating quantum light, as well as a series of demonstrations of the use of metamaterials in quantum optical applications.

© 2025 Author(s). All article content, except where otherwise noted, is licensed under a Creative Commons Attribution-NonCommercial 4.0 International (CC BY-NC) license (<https://creativecommons.org/licenses/by-nc/4.0/>). <https://doi.org/10.1063/5.0216714>

## TABLE OF CONTENTS

I. INTRODUCTION.....	1	B. Spectral domain.....	12
II. THEORETICAL BACKGROUND.....	3	C. Hyperentanglement.....	12
III. PHASE MATCHING CONSIDERATIONS AND FABRICATION METHODS.....	5	VI. SUMMARY AND OUTLOOK.....	12
A. Birefringent phase matching and quasi-phase-matching.....	5		
B. Modulation of the nonlinear coefficient and electric field poling.....	6		
C. 3D laser-induced poling.....	6		
D. Waveguides and metasurfaces.....	6		
IV. SIMULATING SPDC.....	7		
A. Spatial domain.....	8		
B. Spectral domain.....	8		
C. Inverse design.....	9		
V. APPLICATIONS OF QUANTUM LIGHT GENERATED BY SHAPED LIGHT AND STRUCTURED CRYSTALS.....	10		
A. Spatial domain.....	10		

## I. INTRODUCTION

The nonlinear process of spontaneous parametric downconversion (SPDC) is a key method for generating different types of quantum light. Typically, a strong pump source, with frequency and wave vector  $\omega_p, \vec{k}_p$  is sent to a nonlinear crystal, where it can be spontaneously split into two photons, called signal and idler, with corresponding frequencies  $\omega_s, \omega_i$  and wavevectors  $\vec{k}_s, \vec{k}_i$ . For an efficient process, energy conservation ( $\omega_p = \omega_s + \omega_i$ ) and momentum conservation ( $\vec{k}_p = \vec{k}_s + \vec{k}_i + \vec{k}_c$ ) need to be satisfied, where  $\vec{k}_c$  is a possible contribution to the momentum by the nonlinear crystal.

There are several interesting types of quantum light that can be generated by SPDC, including heralded single photon generation, generation of fixed photon number (Fock) states, generation of entangled

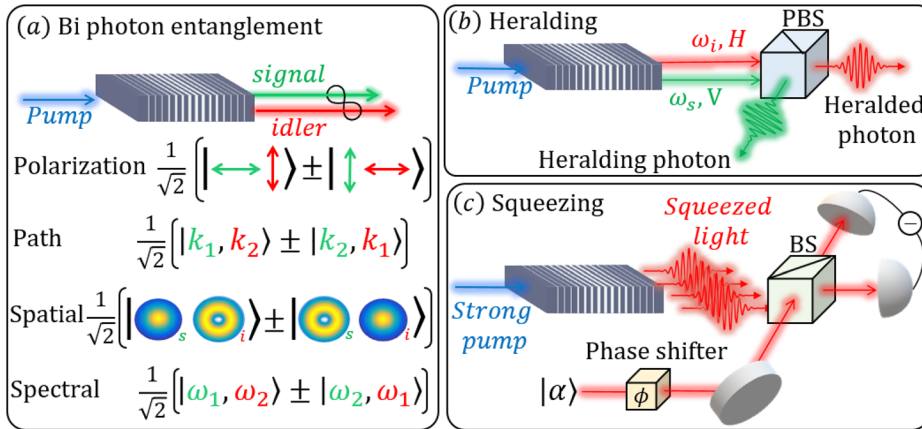


**FIG. 1.** (a) Examples of entanglement created in a type II SPDC process using structured NLPCs. (b) Generation of a heralding signal that indicates the successful occurrence of a quantum event. Heralding involves the detection of one photon (heralded photon) to signal the presence of its entangled partner in a specific state. PBS, polarizing beam splitter, H and V mark the different polarization directions. (c) Squeezed light is generated by propagating a strong pump field through the NLPC. The phase dependent squeezing can be revealed by interfering it with a coherent state  $|\alpha\rangle$ , which serves as a local oscillator. BS, beam splitter.

bi-photon states, and generation of single-mode and two-mode squeezed light, see Fig. 1. In the case of heralded single-photon generation, one of the photons (say the idler photon) is detected, thus heralding the presence of the single photon (the signal) in a different path, see Fig. 1(b). Another option is to use the correlation between the two photons in order to obtain an entangled source. The entanglement can be in many possible degrees of freedom (DOF) of the light, such as polarization, path, spectrum, time, shape, and orbital angular momentum (OAM), see Fig. 1(a). Higher nonlinear coupling, which can be reached, for example, by increasing the pump power or inserting the nonlinear crystal into a resonant cavity, would lead to the generation of squeezed light, see Fig. 1(c).

Let us consider as an example a polarization entangled source, which can be expressed as<sup>1</sup>

$$|\psi\rangle = (|H_a V_b\rangle + e^{i\phi} |V_a H_b\rangle) / \sqrt{2}. \quad (1)$$

This means we have two photons in two paths, labeled “a” and “b.” The SPDC state is a superposition of two possibilities—an H-polarized photon in path “a” and a V-polarized photon in path “b,” or vice versa. The intriguing property of this state is that it is sufficient to perform a polarization measurement on only one of the two photons in order to determine the polarization of the second photon. This property holds even if the two photons are very far apart. As an example, if the result of the measurement is that the photon in path “a” is V-polarized, it means that the photon in path “b” must be H-polarized. In addition, depending on  $\phi$  (i.e., 0 or  $\pi$ ),  $|\psi\rangle$  represents two different Bell states, which are key resources in various quantum information protocols.

In order to generate polarization-entangled photons, a type II nonlinear process is typically used. In this process, the generated signal and idler have orthogonal polarization. As an example, birefringent phase matching can be employed in the nonlinear crystal beta barium borate (BBO), where the specific choice of the crystal cut and the interacting wavelengths leads to the generation of two emission cones, one for the H polarization and the other for the V polarization.<sup>2</sup> These two cones intersect at two points, so that if the light is collected only from these two intersection points, we obtain the desired polarization entanglement. Hence, the generation of polarization-entangled photons can be achieved by clever choice of standard nonlinear crystals and optical configuration. However, the polarization degree of freedom spans only a two-dimensional Hilbert space. Hence, there is a desire to utilize

other degrees of freedom of light, such as spatial or spectral shape, allowing for higher-dimensional operations. The higher dimensionality provides several important advantages, such as the ability to transmit more information on a single photon [ $\log_2(d)$  bit per photon for a  $d$  – dimensional qudit, vs 1 bit photon for two – dimensional qubit] and improved security in quantum key distribution systems.<sup>3,4</sup> However, in the case of high-dimensional states, it is much more difficult to generate the desired state directly, and it usually requires two steps. First, signal and idler photons are generated, and then an optical setup encodes the desired information. It should be emphasized that information encoding is a separate step that requires additional optical elements, such as lenses, filters, beam-splitters, and passive or active masks, before or after the nonlinear crystal.

In this review paper, we discuss another possibility of encoding the desired information into the nonlinear crystal that generates the quantum light. Rather than using a standard nonlinear crystal, together with an optical setup with multiple elements before or after the crystal, we consider functional crystals whereby the nonlinear coefficient is modulated to directly generate the desired quantum states. The crystal, thus, serves as a quantum nonlinear metamaterial so that when it is illuminated by a pump beam, the signal and idler beams with desired spectral and/or spatial correlations will be generated (see Fig. 2). In this sense, the entire optical setup that is required to generate the desired quantum source is replaced by a single nonlinear metamaterial. The realization of these nonlinear metamaterials require several key ingredients: (i) The use of efficient SPDC simulators and machine learning tools for engineering the generation of the different quantum states<sup>5,6</sup> and (ii) new capabilities of shaping the nonlinear coefficient, based on laser-induced poling<sup>7–9</sup> and on advancements in electric field poling.<sup>10</sup> While this ability is mainly used nowadays for periodic modulation, in order to satisfy the momentum conservation condition by quasi-phase-matching, it is possible to go beyond this standard modulation and vary the modulation period, the duty cycle, and the phase of the modulation pattern along the crystal. In fact, structured nonlinear crystals have already been used for more than a decade for spatial<sup>11–16</sup> and spectral<sup>17,18</sup> shaping of light beams in classical nonlinear interactions. Here, we will show that structured nonlinear crystals can also be used in SPDC processes in order to shape the correlations between the signal and idler waves. This review can interest any researcher who uses quantum light, with the intent of familiarize the optics

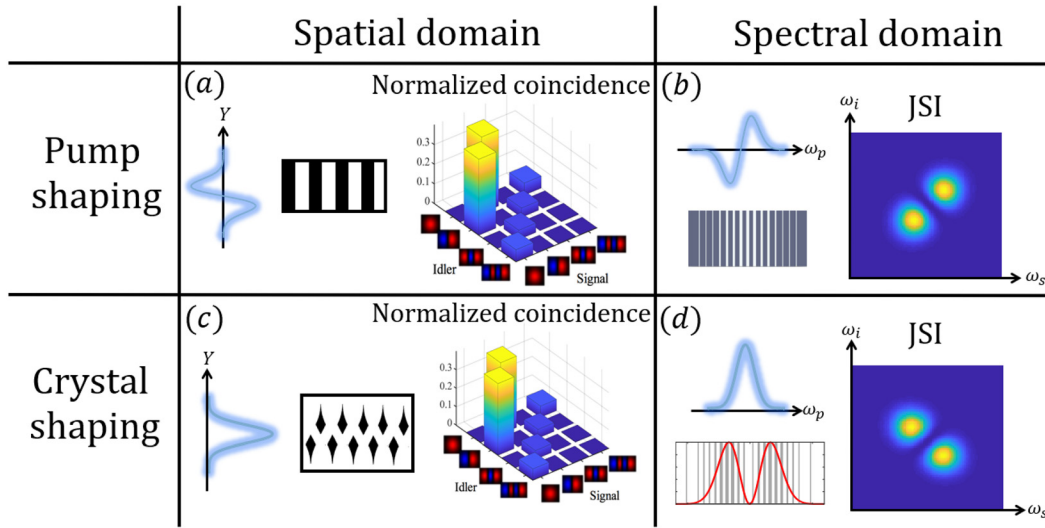


**FIG. 2.** Pump shaping vs crystal shaping in various degrees of freedom. (a) Engineering the spatial correlations between different spatial HG modes using pump shaping. (b) Engineering the JSI using pump shaping. (c) Engineering the spatial correlations between different spatial HG modes using crystal shaping. (d) Engineering the JSI using crystal shaping.

community to the versatile use of spatially engineered bulk nonlinear media for quantum light generation. We give special emphasis on the design of the aforementioned nonlinear structures, with a brief overview of current state of the art fabrication process.

The structure of the paper is as follows: In Sec. II, we derive the evolution of the signal and idler states under the nonlinear Hamiltonian. In Sec. III, we discuss phase matching options, based on crystal birefringence or quasi-phase-matching, as well as fabrication methods to realize the latter, using electric field poling or laser-induced poling. We also briefly review the status of waveguides and metasurfaces for generation of quantum light. Simulation of SPDC, either in the spatial domain or in the spectral domain is discussed in Sec. IV. This section also discusses inverse solving methods. Section V covers applications of quantum light, generated by structured crystals as well as shaped pump beams. Finally, Sec. VI summarizes this review and presents outlook for future studies.

## II. THEORETICAL BACKGROUND

This section will review the theoretical background in order to evaluate SPDC's quantum light properties. We start with the nonlinear Hamiltonian of the following form:<sup>19,20</sup>

$$\hat{H}(t) = \epsilon_0 \int_V dV \chi^{(2)}(\mathbf{r}) \hat{\mathcal{E}}_p(t, \mathbf{r}) \hat{\mathcal{E}}_i^-(t, \mathbf{r}) \hat{\mathcal{E}}_s^-(t, \mathbf{r}) + \text{h.c.}, \quad (2)$$

where  $\epsilon_0$  is the vacuum permittivity,  $\chi^{(2)}$  is the nonlinear second-order susceptibility coefficient,  $V$  is the interaction volume,  $\mathcal{E}_p$  is the undepleted pump field, and  $\hat{\mathcal{E}}_{i/s}^-$  is the quantized electric field operator of the signal and idler photons. Here, we mainly focus on nearly transparent dielectric materials, i.e., at optical frequencies that are far from any electronic resonance of the crystal. In this case, the material nonlinearity in non-centro-symmetric materials can be either modeled as a classical anharmonic oscillator, or using semi-classical quantum mechanical perturbation theory.<sup>21</sup> Since the pump, signal, and idler

electric fields are three-dimensional vectors, the second-order order susceptibility tensor includes  $3 \times 3 \times 3 = 27$  elements, but by using symmetry properties,<sup>21</sup> it can be represented in a contracted notation using only  $3 \times 6 = 18$  elements. Moreover, in a typical nonlinear interaction, only a certain specific setting of the polarizations of the three interacting fields provides phase matching; hence, only one of these 18 elements may need to be used. We note that in previous treatments,<sup>19</sup> the nonlinearity is space independent and can be written outside the integral of Eq. (2). However, these treatments neglect the spatial dependence of the nonlinearity, which allows engineering the signal and idler correlations in various degrees of freedom. Classical fields are defined as follows (for the pump field):<sup>19,20</sup>

$$\mathcal{E}_p(t, \mathbf{r}) = \frac{\mathbf{e}_p}{(2\pi)^{3/2}} \int d\omega d\mathbf{q} \mathcal{E}_p(\omega, \mathbf{q}, z) \exp(ik_{pz}z + i\mathbf{q} \cdot \mathbf{r}_\perp - i\omega t), \quad (3)$$

where  $\mathbf{r}_\perp$  is the transverse coordinate,  $\mathbf{q}$  is the transverse wave vectors,  $\omega$  is the field's angular frequency,  $\mathcal{E}_p(\omega, \mathbf{q})$  is the spatial mode in transverse coordinates,  $k_{pz}$  is the wave vector component in the “z” direction, and  $\mathbf{e}_p$  is the polarization vector of the pump field. Quantized fields are defined similarly as<sup>19,20</sup>

$$\hat{\mathcal{E}}_i(t, \mathbf{r}) = \frac{i\mathbf{e}_i}{(2\pi)^{3/2}} \int d\omega d\mathbf{q} f(\omega) \hat{a}_i(\omega, \mathbf{q}, z) \exp(ik_{iz}z + i\mathbf{q} \cdot \mathbf{r}_\perp - i\omega t), \quad (4)$$

where  $\hat{a}$  is the annihilation operator, and  $f(\omega) = \sqrt{\hbar\omega/2\epsilon_0 c n_i(\omega)}$ . For each of the waves, the dispersion relation sets the relation between the wavevector and angular frequency,  $|\mathbf{q}|^2 + k_z^2 = n^2 \omega^2 / c^2$ . In the Schrödinger picture, the signal and idler state at time  $t$  can be written as

$$|\Psi(t)\rangle = \exp\left[-\frac{i}{\hbar} \int_0^t \hat{H}(t') dt'\right] |0\rangle_s |0\rangle_i. \quad (5)$$

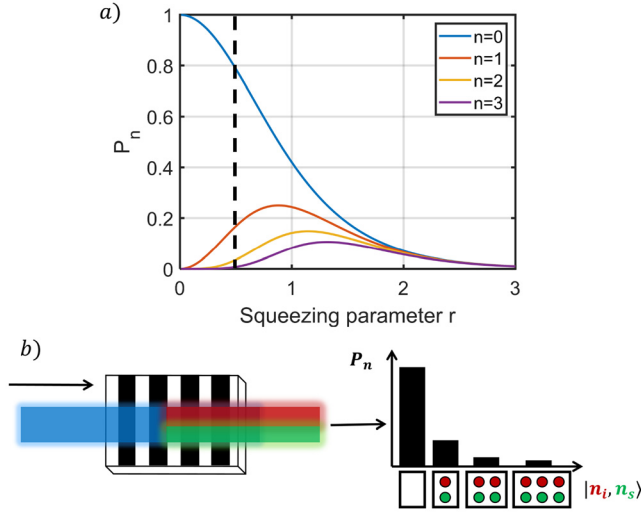


**FIG. 3.** (a) Probability of emitting the signal and idler photons  $|n_s\rangle|n_i\rangle$  as a function of the squeezing parameter  $r$  during SPDC, demonstrating the regime for signal-idler pair emission. (b) The output of squeezed light probabilities is according to the dashed black line. In this case, the probability of emitting three or more photon pairs is negligible.

By writing the RHS of the former equation as a Taylor expansion, we arrive at

$$|\Psi\rangle = \sqrt{1-\lambda} \left( |0\rangle_s |0\rangle_i + \lambda^{1/2} |1\rangle_s |1\rangle_i + \lambda^{2/2} |2\rangle_s |2\rangle_i + \lambda^{3/2} |3\rangle_s |3\rangle_i + \dots \right), \quad (6)$$

where  $\lambda = \tan^2(r)$  and  $r$  is the squeezing parameter.<sup>22</sup> The probabilities to create each order of photon pairs is shown in Fig. 3. For  $r \ll 1$ , the probability of emitting a pair of photons is significantly higher than the probability of emitting higher-order photon pairs. This is the operating regime for generation of heralded single photons and entangled bi-photons since the (unwanted) higher-order photon pairs deteriorate the purity of the generated state. As  $r$  increases, the probabilities of generating  $|n\rangle_s |n\rangle_i$  for  $n > 1$  increases, therefore approaching the bright squeezed vacuum regime.

Assuming the pump power is weak (Fig. 3), all the higher order terms in Eq. (6) can be neglected, and we are left only with the vacuum state and the state having a single signal photon and single idler photon,  $\lambda^{1/2} |1\rangle_s |1\rangle_i$ . We can now plug Eqs. (3) and (4) to Eq. (2). Moreover, we now write the spatial and spectral dependence of the pump field as  $\mathcal{E}_p(\omega, q, z) = B_p(\mathbf{q}_p)S(\omega_p)$ , where  $S$  and  $B_p$  are the spectral and spatial functions of the pump field  $\mathcal{E}_p$ , respectively, assuming no “ $z$ ” dependence of the pump field. The evolution of  $\lambda^{1/2} |1\rangle_s |1\rangle_i$  now becomes

$$\begin{aligned} & \frac{\epsilon_0 \mathbf{e}_p \mathbf{e}_s \mathbf{e}_i}{(2\pi)^3} \int d\omega_p d\omega_s d\omega_i d\mathbf{q}_s d\mathbf{q}_i d\mathbf{q}_p \times S(\omega_p) f_p f_s f_i \\ & \times \int_0^t dt e^{i(\omega_p - \omega_s - \omega_i)t} \int_{-\infty}^{\infty} dx e^{i(k_{px} - k_{sx} - k_{ix})x} \int_{-\infty}^{\infty} dy e^{i(k_{py} - k_{sy} - k_{iy})y} \\ & \times \int_{-\frac{L}{2}}^{\frac{L}{2}} dz B_p(\mathbf{q}_p) \chi^{(2)}(\mathbf{r}) e^{i(k_{pz} - k_{sz} - k_{iz})z} |\mathbf{q}_s, \omega_s\rangle |\mathbf{q}_i, \omega_i\rangle. \end{aligned} \quad (7)$$

Here,  $|\mathbf{q}_s, \omega_s\rangle |\mathbf{q}_i, \omega_i\rangle$  means that we have a signal photon with spatial transverse frequency  $\mathbf{q}_s$  and angular frequency  $\omega_s$ , and an idler photon with spatial transverse frequency  $\mathbf{q}_i$  and angular frequency  $\omega_i$ . We assume that we can extend the boundaries of the time integral

$$\int_{-\infty}^{+\infty} dt e^{i(\omega_p - \omega_s - \omega_i)t} = 2\pi \delta(\omega_p - \omega_s - \omega_i). \quad (8)$$

This expression is a manifestation of the energy conservation of the SPDC process. Similar to Ref. 19, we can now integrate over the pump frequency, which owing to the energy conservation relation means that  $\omega_p$  is replaced with  $\omega_s + \omega_i$ ,

$$\begin{aligned} & \int d\omega_s d\omega_i d\mathbf{q}_s d\mathbf{q}_i d\mathbf{q}_p \times S(\omega_s + \omega_i) f_p f_s f_i \\ & \times \int_{-\infty}^{\infty} dx e^{i(k_{px} - k_{sx} - k_{ix})x} \int_{-\infty}^{\infty} dy e^{i(k_{py} - k_{sy} - k_{iy})y} \\ & \times \int_{-\frac{L}{2}}^{\frac{L}{2}} dz B_p(\mathbf{q}_p) \chi^{(2)}(\mathbf{r}) e^{i(k_{pz} - k_{sz} - k_{iz})z} |\mathbf{q}_s, \omega_s\rangle |\mathbf{q}_i, \omega_i\rangle. \end{aligned} \quad (9)$$

We note that every  $k$  component written in Eq. (9) is frequency dependent and is omitted for brevity. Equation (9) can now be solved either numerically or, sometimes, analytically. Importantly, although this equation can give valuable information about the basic correlations between different degrees of freedom, it does not take into account diffraction and high-order contributions [Eq. (6)]. Therefore, a more general numerical solution is needed, given in Sec. IV A few assumptions can help us to further simplify the result. Assuming  $\chi^{(2)}(r) = \chi^{(2)} d(z)$ , we can integrate over the transverse coordinates  $x$  and  $y$ . This dictates a transverse momentum condition,  $\mathbf{q}_p = \mathbf{q}_s + \mathbf{q}_i$ , hence integrating over  $\mathbf{q}_p$  we reach

$$\begin{aligned} |\Psi(t)\rangle & \propto \sqrt{1-\lambda} |0\rangle_s |0\rangle_i + \sqrt{\lambda} \chi^{(2)} \int d\omega_s d\omega_i d\mathbf{q}_s d\mathbf{q}_i \\ & \times f_p f_s f_i S(\omega_s + \omega_i) B_p(\mathbf{q}_s + \mathbf{q}_i) \Phi(\omega_i, \omega_s) |\mathbf{q}_s, \omega_s\rangle |\mathbf{q}_i, \omega_i\rangle. \end{aligned} \quad (10)$$

Here,  $\Phi(\omega_i, \omega_s)$  is the phase matching function, which depends solely on the parameters of the nonlinear crystal

$$\Phi(\omega_i, \omega_s) = \int_{-\frac{L}{2}}^{\frac{L}{2}} dz d(z) e^{i(k_{pz}(\omega_i + \omega_s) - k_{sz}(\omega_s) - k_{iz}(\omega_i))z}. \quad (11)$$

If the nonlinearity is constant along the crystal, its dimensionless and normalized function is  $d(z) = 1$ , but we can also consider space-dependent nonlinearity, which is employed in the case of quasi-phase-matching, as will be discussed in Sec. III. As an example, if the nonlinearity is periodically modulated with a period  $\Lambda$ , then  $d(z) = \text{sign}[\cos(2\pi z/\Lambda)]$ . The result of Eq. (10) presents the main contributions to the generated SPDC state: the pump spectral function,  $S(\omega_s + \omega_i)$ , the pump spatial function,  $B_p(\mathbf{q}_s + \mathbf{q}_i)$ , and the crystal phase matching function,  $\Phi(\omega_i, \omega_s)$ . We further note that in the plane wave approximation, the pump spatial function is  $\delta(\mathbf{q}_p)$ ; hence, the transverse phase matching condition becomes  $\mathbf{q}_s = -\mathbf{q}_i$ . Moreover, for a collinear interaction in which all the waves are assumed to be plane waves, the pump spatial function can be ignored, and the



generated SPDC state is governed by the so-called joint spectral amplitude (JSA), which is given as

$$\text{JSA}(\omega_i, \omega_s) \approx S(\omega_s + \omega_i) \times \Phi(\omega_i, \omega_s), \quad (12)$$

and the SPDC state attains a simple form as

$$|\Psi(t)\rangle \propto \sqrt{1-\lambda}|0\rangle_s|0\rangle_i + \sqrt{\lambda}\chi^{(2)} \int d\omega_s d\omega_i f_p f_s f_i \text{JSA}(\omega_i, \omega_s) |\omega_s\rangle |\omega_i\rangle. \quad (13)$$

We emphasize that this result was obtained only after several approximations were made, and in particular, we assumed that we can take only the first two terms in the Taylor expansion of Eq. (6). In order to include higher order terms, it is necessary to use numerical methods, as will be discussed in Sec. IV.

### III. PHASE MATCHING CONSIDERATIONS AND FABRICATION METHODS

Two of the most important implications of the derivation in Sec. II are the requirements for momentum and energy conservation. In the SPDC process, these conservation laws shape the entangled photon state. Energy conservation ensures that the combined energy of the resulting signal and idler photons equals that of the incoming pump photon, determining their wavelengths. Simultaneously, momentum conservation dictates that the total momentum remains constant. This dual conservation requirement enables shaping the signal-idler correlations for different degrees of freedom of light. Here, we will review the two main methods to achieve phase matching—birefringent phase matching and quasi-phase-matching (QPM). The latter requires means of modulating the nonlinear coefficient, and we will review two methods to achieve it—electric field poling of ferroelectrics and laser-induced poling. We will also briefly review two other platforms used in generating quantum light—optical waveguides and metasurfaces.

#### A. Birefringent phase matching and quasi-phase-matching

SPDC requires conserving the photon momenta in the process, or in other words, satisfying the phase matching condition,  $\vec{k}_p = \vec{k}_s + \vec{k}_i + \vec{k}_c$ . There are two main methods to achieve this: birefringent phase matching and quasi-phase-matching. The traditional method relies on the birefringence of nonlinear crystals. There are two types of birefringent crystals. The first are uniaxial crystals (such as LiNbO<sub>3</sub> or LiTaO<sub>3</sub>) in which the refractive index along two crystallographic axes—X and Y—is identical and is called the ordinary index  $n_o$ , and is different with respect to the extraordinary index along the optical axis, or Z axis,  $n_z$ . In the second group of known as biaxial crystals, the refractive index is different in every direction. Important examples are KTiOPO<sub>4</sub>, KTiAsO<sub>4</sub>, RbTiAsO<sub>4</sub>, and RbTiOPO<sub>4</sub>, but it should be noted that also for these crystals, the refractive indices in the X and Y directions are relatively similar, and are quite different with respect to  $n_z$ . In order to satisfy the phase-matching condition, one needs to find the correct propagation angles and crystal temperatures. Specifically, the refractive index at an angle  $\theta$  with respect to the optical axis, denoted  $n_{ex}(\theta)$  is given by<sup>21</sup>

$$\frac{1}{n_{ex}(\theta)^2} = \frac{\sin^2(\theta)}{n_z^2} + \frac{\cos^2(\theta)}{n_o^2}. \quad (14)$$

As can be seen,  $n_{ex}(\theta)$  can attain any value between  $n_o$  and  $n_z$  by varying the angle  $\theta$  between 0 and  $\pi/2$ . Hence, by using the dependence of refractive index on angle, polarization, and temperature, it is often possible to satisfy the phase matching conditions and obtain creative configurations for SPDC, see for example, Ref. 2. However, birefringent phase matching is limited in several key aspects. It is not always possible to find the required phase matching conditions, since they depend on the given dispersion of the nonlinear crystal. In addition, since the interacting waves must be polarized along different directions, only non-diagonal terms of the  $\chi^{(2)}$  tensor can be used. They are usually smaller with respect to diagonal elements, and in particular, with respect to the largest element,  $\chi_{33}^{(2)}$ . The efficiency may also be reduced owing to the walk-off between the interacting beams.

These problems can be solved by quasi-phase-matching (QPM),<sup>23</sup> which is based on modulating the nonlinear coefficient of the crystal along the interaction path. In its simplest form, QPM is obtained by periodic one-dimensional modulation of the nonlinear coefficient, with a period  $\Lambda$ . For binary (positive and negative) modulation, with a duty cycle of 0.5, the nonlinear coefficient can be written as

$$\chi_{eff}^{(2)}(z) = \chi_{ij}^{(2)} \sum_{m=-\infty}^{\infty} \frac{2}{\pi m} \sin\left(\frac{\pi m}{2}\right) e^{-\frac{i\pi m}{\Lambda} z}. \quad (15)$$

From the Fourier series decomposition, it is easy to see that this modulation provides  $z$ -dependent phase terms at odd integer multiples of  $2\pi/\Lambda$  that can be used for phase matching. The highest efficiency is obtained for first-order QPM,  $m = 1$ , and in that case, the material's second-order tensor element  $\chi_{ij}^{(2)}$  is multiplied by the Fourier coefficient  $2/\pi$ . Owing to the dispersion of the nonlinear crystal, if phase matching is satisfied for one order, the phase mismatch is typically very large for all the other orders. Hence, their effect can be ignored.

The key advantage here is that the phase matching is no longer limited by the crystal's dispersion and birefringence properties and can be satisfied by selecting the modulation period  $\Lambda$ . Moreover, the process can be designed so that all the interacting waves have the same polarization, thus enabling the benefit of the large diagonal elements of the  $\chi^{(2)}$  tensor. As an example, if all the waves are polarized along the Z axis of LiNbO<sub>3</sub>, the relevant nonlinear tensor element is  $\chi_{33}^{(2)}$ . It is interesting to note that even though the effective nonlinear coefficient is reduced by  $2/\pi$  for first-order QPM, there is still significant improvement in efficiency with respect to a birefringent phase matching process. For example, if the two waves are polarized along the X direction to generate a nonlinear polarization term along the Z direction, the relevant tensor element is  $\chi_{31}^{(2)}$  and the improvement in efficiency in the case of QPM is  $[(2/\pi)\chi_{33}^{(2)}/\chi_{31}^{(2)}]^2 \approx 20$ .

Moreover, QPM is not limited to periodic modulation of the nonlinear coefficient in one dimension. Specifically, it is possible to periodically modulate the nonlinear coefficient in two- or three-dimensions<sup>24–26</sup> and to extend the modulation toward quasiperiodic modulations.<sup>27–29</sup> Quasiperiodic poling enables the simultaneous phase matching of several interactions. Moreover, increase or decrease in the modulation period along the interaction<sup>30,31</sup> allows for broadband adiabatic frequency conversion. This flexibility is also very useful for designing SPDC interactions, as will be outlined in Secs. III B–III D and V.

## B. Modulation of the nonlinear coefficient and electric field poling

QPM relies on the ability to spatially modulate the nonlinear coefficient with micrometer-scale resolution. Several methods were studied in the past for that, including ion exchange,<sup>32</sup> irradiation with electron beams,<sup>33</sup> and laser-induced domain inversion<sup>34</sup> (more on this in Sec. III C), but in the last three decades, the dominant method for that is electric field poling of ferroelectric crystals.<sup>35</sup> This method relies on the delivery of a high-voltage pulse through structured electrodes. When the applied electric field surpasses the coercive threshold of the ferroelectric crystal, it leads to an inversion of the electrical dipole's alignment within the areas marked by the electrodes. Consequently, this leads to a permanent binary alteration of the second-order susceptibility, and the poled shape follows the arrangement of the electrodes, see Fig. 4(a).

Electric field poling is now widely used with LiNbO<sub>3</sub>, LiTaO<sub>3</sub>, and KTiOPO<sub>4</sub>, and periodically poled crystals are available commercially from several vendors. The typical crystal dimensions are a thickness of 0.5–1 mm, length of 10–40 mm, and poling periods of 5–40 μm, but state of the art values include thickness of up to 10 mm (Ref. 36) and poling periods as small as 317 nm.<sup>37</sup> Since the poling structure is defined by electrodes that are patterned on the plane of the crystal, the poling method is not limited to one-dimensional periodic structures and was extended to chirped,<sup>30,31</sup> quasiperiodic,<sup>27–29</sup> and two-dimensional designs.<sup>24,25</sup>

## C. 3D laser-induced poling

In recent years, another method was demonstrated for modulating the nonlinear coefficient of ferroelectrics, based on point-by-point focusing of an ultrafast laser. This method enables the modulation of the nonlinear coefficient in all three dimensions of the crystal, see Fig. 4(b). There are two variants of the laser-induced modulation. One variant is based on local heating of the crystal at the focal point of the laser. This destroys the crystalline structure at that point, so that the crystal becomes amorphous and the nonlinear coefficient is locally erased. This method was demonstrated for LiNbO<sub>3</sub>.<sup>7</sup> A second variant is based on generating a local temperature gradient at the focal point. Under the right conditions, this gradient locally inverts the spontaneous polarization of the crystal, and therefore inverts the nonlinear

coefficient of the crystal. This method was demonstrated for barium calcium titanate, barium calcium niobate,<sup>8</sup> and recently also for LiNbO<sub>3</sub>.<sup>38</sup> More details on optical poling of ferroelectrics can be found in a recent review article.<sup>9</sup>

Three-dimensional modulation of the nonlinear crystal increases the phase matching options, as the crystal provides reciprocal vectors for phase matching in all three dimensions. This enables new opportunities for nonlinear holography,<sup>13,14</sup> and even for storing and retrieving multiple images in a single nonlinear crystal.<sup>15,16</sup> The typical lengths of 3D poled structures are still much shorter than those achieved by electric field poling, with record length of about 2.6 mm.<sup>39</sup> The typical poling periods are in the range of 10 μm, but the state of the art is as small as 500 nm.<sup>38</sup>

## D. Waveguides and metasurfaces

While this paper focuses primarily on bulk nonlinear metamaterials, we would like to briefly mention other platforms for generating quantum light. Optical waveguides have been studied for many years as nonlinear frequency converters<sup>40</sup> and more specifically for quantum optics applications.<sup>41,42</sup> Here, we mainly consider waveguides that utilize second-order nonlinearity. In lithium niobate, waveguides can be formed by titanium ion-diffusion<sup>43</sup> or proton exchange,<sup>44</sup> whereas in KTiOPO<sub>4</sub> (KTP) they can be formed by Rb-Ba ion exchange.<sup>45,46</sup> In KTP, this process is used to form a segmented waveguide, which simultaneously guides the light and enables QPM.

In recent years, an emerging new platform has been based on wafers of thin film lithium niobate (TFLN).<sup>47</sup> Typically, these wafers have a layer of several hundred nanometers of LiNbO<sub>3</sub> on a lower index SiO<sub>2</sub> substrate. Hence, in comparison to waveguides that are based on ion-diffusion, the TFLN waveguides provide much tighter confinement of the modes, with a smaller waveguide cross-sectional area, thus leading to higher efficiency.

Key advantages of waveguide frequency converters are improved conversion efficiency with respect to bulk crystals, the ability to control the dispersion using the waveguide dimensions, and the possible integration of the frequency converter with other optical devices such as directional couplers and modulators on the same chip. In terms of efficiency, one can compare second harmonic generation in a waveguide with a length  $L$  and cross-sectional area  $A_w$  to a bulk crystal with the same length, where confocal focusing is used. The ratio of efficiencies for the two options is<sup>48</sup>

$$\frac{\eta_{\text{waveguide}}}{\eta_{\text{bulk}}} \approx \frac{\lambda_{\omega} L}{2n_{\omega} A_w}, \quad (16)$$

where  $n_{\omega}$  is the refractive index of the fundamental wave. For a typical interaction length of 1 cm, the improvement in efficiency can reach 2–3 orders of magnitude.

In addition to the high efficiency, optical waveguides offer the possibility of controlling the dispersion of the guided modes, which depends on the waveguide's geometrical parameters.<sup>49</sup> Just as QPM achieved by electric field poling takes care of the phase velocity matching, dispersion engineering can be used to tailor the group velocity matching of the interacting waves. An important application of group velocity matching is to enable efficient conversion of ultrashort pulses, which would otherwise suffer from temporal walkoff between the interacting waves. As for quantum applications, it offers the ability to generate separable signal-idler states in SPDC. In bulk materials, this is

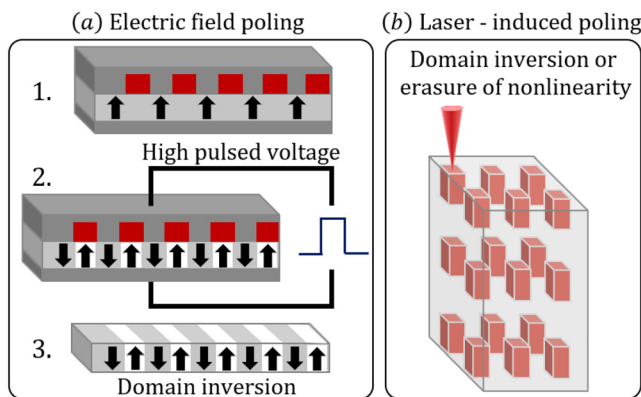


FIG. 4. Poling techniques: (a) electric field poling and (b) laser-induced poling.

possible only for a handful of nonlinear crystals at very specific wavelengths. However, the dispersion engineering that is offered by optical waveguides enables us to reach this condition at any chosen wavelength.<sup>50</sup>

The key limitation of waveguide devices is the power limitation. Since the mode size is of the order of  $1\ \mu\text{m}$ , the intensity can easily surpass the damage threshold of the crystal, even for moderate power levels. However, in quantum optics applications, there is no need to reach high power, in particular since this may lead for unwanted generation of higher order terms, as explained in Sec. II.

Another interesting platform that we would like to briefly mention is surface metamaterials or metasurfaces in short. Surface metamaterials are two-dimensional structures that are typically composed of an array of either metal or dielectric sub-wavelength structures, where the unit cells are commonly referred to as meta-atoms. These devices are characterized for specific wavelengths by strong (resonant) light-matter interaction in each meta-atom and open many interesting possibilities for shaping the wavefront, polarization, and spectrum of light. Moreover, in some cases, by proper selection of the materials and the unit cell structure, new wavelengths can be generated through a nonlinear process.<sup>51</sup> Specifically, SPDC was demonstrated in nonlinear metasurfaces based on GaAs resonant structures on fused silica substrate,<sup>52</sup> on silica resonant structures on thin LiNbO<sub>3</sub> substrate<sup>53</sup> and on plasmonic metasurfaces, using silver stripes on bulk LiNbO<sub>3</sub>.<sup>54</sup> The latter example involves metals that may exhibit significant losses, thus reducing the coherence of the quantum state. Nevertheless, it was shown that the quality of the quantum state is preserved, even for highly absorbing structures, as long as the dephasing time is much longer than the propagation time.<sup>55</sup> This condition can be reached in metasurfaces that are characterized by very short, sub-micron, interaction length. More details can be found in recent reviews on metasurfaces for quantum optics applications.<sup>56,57</sup>

Perhaps the most interesting feature of the nonlinear metasurfaces is the relaxed phase-matching requirement; since the interaction is performed in a very thin structure, resulting in a very short effective interaction length  $L$  in the longitudinal direction, the efficiency, which scales as  $\sin^2(\Delta kL/2)$  can remain high for large longitudinal phase mismatch values  $\Delta k$ . This means that multiple signal-idler pairs, with different wavelengths can be generated. Typically, one of these wavelengths is set by the resonance of the meta-atom, whereas the pump determines the other wavelength via energy conservation. This allows for the generation of different types of cluster states by pumping the metasurface with multiple pump frequencies.<sup>52</sup> The main limitation of metasurfaces for quantum optics application is their relatively low efficiency, owing to the very short interaction length. At present, the typical coincidence rate is at most of a few counts per second; hence, 3–4 orders of magnitude lower with respect to those achieved by bulk devices.

In addition to the generation of quantum light, metasurfaces can also be used for performing unitary transformations between its different degrees of freedom. As examples, liquid-crystal-based Q-plates<sup>58</sup> as well as silicon-based geometric phase metasurfaces<sup>59</sup> were used to couple between the spin and angular degrees of freedom of a single photon.

#### IV. SIMULATING SPDC

In Sec. II, we presented straightforward, closed-form approximations for SPDC applicable to basic scenarios. However, for more

complex situations where the nonlinearity varies arbitrarily within the crystal, diffraction effects are present, higher-order effects need to be considered, or correlations need to be computed alongside the state, numerical solutions are required.<sup>60</sup> This section will outline the numerical methodologies employed for such cases.

In the effort to model the behavior of a pump interacting with nonlinear media, our goal is to develop a simulation tool capable of predicting the output quantum state and the correlations between entangled photons. To achieve this, we adopt the slowly varying envelope approximation for each frequency component independently, following the approach outlined in Ref. 61. The equations of motion, derived from Maxwell's equations<sup>62</sup> and applied to the frequency-dependent field operators<sup>6</sup> under the undepleted coherent pump and slowly varying envelope approximations, are expressed as follows:<sup>6,63</sup>

$$\begin{aligned} & \left( i \frac{\partial}{\partial z} + \frac{\nabla_{\perp}^2}{2k_i(\omega)} \right) \hat{A}_i(\mathbf{r}, \omega) \\ & = - \frac{\omega^2}{c^2 k_i(\omega)} \chi^{(2)}(\mathbf{r}) \int d\omega' e^{-i\Delta k(\omega, \omega')z} A_p(\mathbf{r}, \omega + \omega') \hat{A}_s^*(\mathbf{r}, \omega'). \end{aligned} \quad (17)$$

Here,  $\hat{A}_{i,s}$  represent the idler and signal field operators, respectively, and  $A_p$  is the pump field. The transverse Laplacian is denoted by  $\nabla_{\perp}^2$ ,  $\chi^{(2)}(\mathbf{r})$  represents the second-order susceptibility,  $c$  is the speed of light, and  $k_i(\omega)$  is the idler's wavevector, dependent on the frequency. The term  $\nabla_{\perp}^2$  encapsulates diffraction, while the phase-mismatch  $\Delta k(\omega, \omega')z$  encapsulates dispersion. The same equation can be written for the signal by interchanging “i” with “s” and “s” with “i.” Henceforth, we will use the coupling coefficient  $\kappa_j(\mathbf{r}, \omega) = \frac{\omega^2}{c^2 k_j(\omega)} \chi^{(2)}(\mathbf{r})$ , where  $j = i, s$ .

Examining correlations between entangled photons in quantum optics is a crucial method for characterizing their quantum behavior. Here, we show a generalized method for simulating correlations between photons created via SPDC, in the spatial and spectral domains. The first-order correlation in the case of SPDC can be written as<sup>6,63</sup>

$$G_{\alpha\beta}^{(1)}(\mathbf{r}, t, \mathbf{r}', t') = \langle 0 | \hat{A}_{\alpha}^{\dagger}(\mathbf{r}, t) \hat{A}_{\beta}(\mathbf{r}', t') | 0 \rangle, \quad (18)$$

where  $\alpha, \beta$  represent either the idler or signal. In the spatial domain,<sup>62</sup>  $\hat{A}_{\alpha}(\mathbf{r}) = \sum_{\mathbf{q}} \frac{e^{i\mathbf{q}\cdot\mathbf{r}}}{\sqrt{V}} \hat{a}_{\mathbf{k}_{\alpha}+\mathbf{q}}$  is the paraxial envelope operator around a carrier with a wavevector  $\mathbf{k}_{\alpha}$ , and  $\hat{a}_{\mathbf{k}_{\alpha}+\mathbf{q}}$  is the annihilation operator, annihilating a photon in mode  $\mathbf{k}_{\alpha}+\mathbf{q}$ . In its degenerate form,  $G_{\alpha\alpha}^{(1)}(\mathbf{r}, t, \mathbf{r}, t')$  is the probability of detecting a single photon in mode  $\alpha$  at position and time  $(\mathbf{r}, t)$ . In the spectral domain,  $\hat{A}_{\alpha}(t)$  is the slowly varying-envelope operator. By inserting the identity operator  $I = \sum_{\gamma} |1_{\gamma}\rangle\langle 1_{\gamma}|$ , we write the simplified first-order correlation function as

$$G_{\alpha\beta}^{(1)}(\mathbf{r}, t, \mathbf{r}', t') = \sum_{\gamma} \langle 0 | \hat{A}_{\alpha}^{\dagger}(\mathbf{r}, t) | 1_{\gamma} \rangle \langle 1_{\gamma} | \hat{A}_{\beta}(\mathbf{r}', t') | 0 \rangle, \quad (19)$$

where  $|1_{\gamma}\rangle$  is a single photon state in mode  $\gamma$ . The index  $\gamma$  can represent spatial modes, frequencies, and polarizations. For the spatial domain  $\gamma = k$  whereas for the spectral domain  $\gamma = \Omega_{i,s}$ . In the spectral domain, there is an integral over  $d\Omega$  since we consider a range of frequencies for the pump wave.



A second type of first-order quantum correlation involves terms that are quadratic in the annihilation or creation operators,

$$Q_{\alpha\beta}(\mathbf{r}, t, \mathbf{r}', t') = \langle 0 | \hat{A}_\alpha(\mathbf{r}, t) \hat{A}_\beta(\mathbf{r}', t') | 0 \rangle. \quad (20)$$

We insert again the identity operator and write the simplified function as

$$Q_{\alpha\beta}(\mathbf{r}, t, \mathbf{r}', t') = \sum_\gamma \langle 0 | \hat{A}_\alpha(\mathbf{r}, t) | 1_\gamma \rangle \langle 1_\gamma | \hat{A}_\beta(\mathbf{r}', t') | 0 \rangle. \quad (21)$$

We define four amplitudes or matrix elements as

$$\begin{aligned} A_i^{\text{vac}}(\mathbf{r}, \omega) &\equiv \langle 0 | \hat{A}_i(\mathbf{r}, \omega) | 1_i \rangle, \\ A_i^{\text{out}}(\mathbf{r}, \omega) &\equiv \langle 1_i | \hat{A}_i(\mathbf{r}, \omega) | 0 \rangle, \\ A_s^{\text{vac}}(\mathbf{r}, \omega) &\equiv \langle 0 | \hat{A}_s(\mathbf{r}, \omega) | 1_s \rangle, \\ A_s^{\text{out}}(\mathbf{r}, \omega) &\equiv \langle 1_s | \hat{A}_s(\mathbf{r}, \omega) | 0 \rangle. \end{aligned} \quad (22)$$

We want to solve the dynamics in terms of the amplitudes defined in Eq. (22). Multiplying the Heisenberg equations by  $\langle 1_\gamma |$  from the left and by  $|0\rangle$  from the right, we get

$$\begin{aligned} &\left( i \frac{\partial}{\partial z} + \frac{\nabla_\perp^2}{2k_i(\omega)} \right) \begin{pmatrix} A_i^{\text{out}} \\ A_i^{\text{vac}} \end{pmatrix}(\mathbf{r}, \omega) \\ &= -\kappa_i(\mathbf{r}, \omega) \int d\omega' e^{-i\Delta k(\omega, \omega')z} A_p(\mathbf{r}, \omega + \omega') \begin{pmatrix} A_s^{\text{vac}} \\ A_s^{\text{out}} \end{pmatrix}^*(\mathbf{r}, \omega'), \end{aligned} \quad (23)$$

$$\begin{aligned} &\left( i \frac{\partial}{\partial z} + \frac{\nabla_\perp^2}{2k_s(\omega)} \right) \begin{pmatrix} A_s^{\text{out}} \\ A_s^{\text{vac}} \end{pmatrix}(\mathbf{r}, \omega) \\ &= -\kappa_s(\mathbf{r}, \omega) \times \int d\omega' e^{-i\Delta k(\omega, \omega')z} A_p(\mathbf{r}, \omega + \omega') \begin{pmatrix} A_i^{\text{vac}} \\ A_i^{\text{out}} \end{pmatrix}^*(\mathbf{r}, \omega'). \end{aligned} \quad (24)$$

We solve these four coupled equations under the initial conditions at the beginning of the crystal ( $z = 0$ ),  $A_\alpha^{\text{vac}}(\mathbf{r}, \omega) = 0$ . In principle, Eqs. (23) and (24) can now be solved deterministically. The solution is found in a similar manner to solving coupled wave equations in classical nonlinear optics, using for example the method of split-step Fourier.<sup>64</sup> This approach is valid and may be efficient when the number of modes supported by the system is small. This numerical method partitions propagation through the nonlinear medium into steps small enough to allow independent evaluation of linear effects resulting from the dispersion characteristics of the medium, and nonlinear effects describing the nonlinear interactions introduced by the medium. Solving in this independent iterative manner results in a numerical solution to an equation with no general analytic solution. The method involves the calculation of the effects of the linear operator in the spatial frequency domain, and the nonlinear operator in the spatial domain, requiring the application of the fast Fourier transform (FFT) and inverse FFT with every step. Assuming transverse crystal dimensions  $N * N$ , computationally the method requires  $z/dz$  FFT operations over the two-dimensional transverse plane, requiring  $z/dz * \mathcal{O}(N^2 \log N)$  operations. Additionally, as an increasing step size results in a higher approximation error, achieving good numerical solutions can be computationally expensive.

The second-order correlation function,  $G_{\alpha\beta\beta\alpha}^{(2)}(\gamma, \gamma'; \gamma', \gamma)$ , represents the probability of detecting one photon in mode  $\gamma$  and another in mode  $\gamma'$ . Experimentally, this quantity corresponds to the coincidence rate between these two photons. Specifically, we can express this as

$$\begin{aligned} G_{\alpha\beta\beta\alpha}^{(2)}(\gamma, \gamma'; \gamma', \gamma) &= \langle \hat{A}_\alpha^\dagger(\gamma) \hat{A}_\alpha(\gamma) \rangle \langle \hat{A}_\beta^\dagger(\gamma') \hat{A}_\beta(\gamma') \rangle \\ &\quad + |\langle \hat{A}_\alpha^\dagger(\gamma) \hat{A}_\beta(\gamma') \rangle|^2 + |\langle \hat{A}_\alpha(\gamma) \hat{A}_\beta^\dagger(\gamma') \rangle|^2 \\ &= G_{\alpha\alpha}^{(1)}(\gamma, \gamma) G_{\beta\beta}^{(1)}(\gamma', \gamma') + |G_{\alpha\beta}^{(1)}(\gamma, \gamma')|^2 + |Q_{\alpha\beta}(\gamma, \gamma')|^2. \end{aligned} \quad (25)$$

Given the quadratic nature of the Hamiltonian of SPDC and the Gaussian essence of the vacuum state, the resulting output state also adopts a Gaussian form. Notably, all higher-order moments can be derived from the linear and quadratic moments.<sup>5,6</sup> This was used in the derivation shown in Eq. (25).

### A. Spatial domain

Spatially entangled photons offer a unique avenue for exploring high-dimensional entanglement, an area of significant interest in quantum information. Their potential for high-density encoding of quantum information has drawn considerable attention. Numerous studies have delved into the spatial correlations exhibited by entangled photon pairs.<sup>5,6,65–69</sup> This interest has been fueled by the discovery of novel applications that capitalize on the quantum properties of these photons for tasks like image processing and multichannel operations.

In this section, we make two primary assumptions. First, we consider a CW pump. In the case of a CW pump, the pump field is assumed to have the form  $A_p(\mathbf{r}, \omega + \omega') = A_p(\mathbf{r}) \delta(\omega - \omega_p)$ . Second, we assume that both the idler and signal undergo postselection through narrow spectral filters. These assumptions simplify the coupled Heisenberg equations, resulting in the following expressions:<sup>6</sup>

$$\left( i \frac{\partial}{\partial z} + \frac{\nabla_\perp^2}{2k_i} \right) \begin{pmatrix} A_i^{\text{out}} \\ A_i^{\text{vac}} \end{pmatrix} = -\kappa_i(\mathbf{r}) e^{-i\Delta k z} A_p(\mathbf{r}) \begin{pmatrix} A_s^{\text{vac}} \\ A_s^{\text{out}} \end{pmatrix}^*, \quad (26)$$

$$\left( i \frac{\partial}{\partial z} + \frac{\nabla_\perp^2}{2k_s} \right) \begin{pmatrix} A_s^{\text{out}} \\ A_s^{\text{vac}} \end{pmatrix} = -\kappa_s(\mathbf{r}) e^{-i\Delta k z} A_p(\mathbf{r}) \begin{pmatrix} A_i^{\text{vac}} \\ A_i^{\text{out}} \end{pmatrix}^*. \quad (27)$$

In principle, the solution to Eqs. (26) and (27) can be determined by scanning over all potential modes and their corresponding mode envelopes as boundary conditions. This method is valid and can be efficient when the system supports a small number of modes. However, employing a stochastic boundary condition can be more efficient when dealing with a continuum of transverse modes, as demonstrated in Refs. 5, 6, and 61. In that case, rather than calculating separately for each plane wave mode, one can define “noise modes,” which are superpositions of single photon modes with different wavevectors, where each mode has an random phase.

### B. Spectral domain

As we discussed in Sec. II [see Eq. (12)], a commonly employed approximation for the joint spectral intensity (JSI)<sup>70</sup> is  $JSI = |JSA|^2 = |S(\omega + \omega') \Phi(\omega, \omega')|^2$ . This approximation is derived through first-order perturbation theory. As a reminder,  $S(\omega + \omega')$  is the spectral profile of the pump laser, and  $\Phi(\omega, \omega')$  denotes the phase-matching function, see Eq. (11). It is important to note that this approximation

relies on the assumption that the joint spectral properties of entangled photon pairs are exclusively influenced by the spectral characteristics of the pump laser and its interaction with the nonlinear crystal responsible for generating the photon pairs.

However, caution is warranted as this approximation may not always be accurate. While it serves as a convenient and often useful model for comprehending joint spectral characteristics, its limitations become apparent, particularly when confronted with specific experimental conditions or nuanced crystal properties that this simplified approach might not adequately represent.

In this section, we assume plane waves; thus, the term  $\frac{\nabla^2}{2k}$  disappears. This simplifies the coupled Heisenberg equations [see Eqs. (23) and (24)], resulting in the following expressions:<sup>63</sup>

$$i \frac{\partial}{\partial z} \begin{pmatrix} A_{i,\Omega}^{\text{out}} \\ A_{i,\Omega}^{\text{vac}} \end{pmatrix} (z, \omega) = -\kappa_i(\omega, z) \int d\omega' e^{i\Delta k(\omega, \omega')z} A_p(\omega + \omega') \times \begin{pmatrix} A_{s,\Omega}^{\text{vac}} \\ A_{s,\Omega}^{\text{out}} \end{pmatrix}^* (z, \omega'),$$

$$i \frac{\partial}{\partial z} \begin{pmatrix} A_{s,\Omega}^{\text{out}} \\ A_{s,\Omega}^{\text{vac}} \end{pmatrix} (z, \omega) = -\kappa_s(\omega, z) \int d\omega' e^{i\Delta k(\omega, \omega')z} A_p(\omega + \omega') \times \begin{pmatrix} A_{i,\Omega}^{\text{vac}} \\ A_{i,\Omega}^{\text{out}} \end{pmatrix}^* (z, \omega'). \quad (28)$$

Now we write the first-order correlations at the end of the crystal,  $z = L$ , considering all frequencies  $\Omega$ ,

$$G_{z\beta}^{(1)}(\omega, \omega') = \delta_{z,\beta} \int d\Omega A_{z,\Omega}^{\text{out}*}(L, \omega) A_{\beta,\Omega}^{\text{out}}(L, \omega'), \quad (29)$$

where the Kronecker delta in Eq. (29) arises due to the vanishing photon amplitudes other than those appearing in Eq. (22), implying that  $G_{is}^{(1)} = G_{si}^{(1)} = 0$ . The second type of first-order quantum correlation will take the form of

$$Q_{z\beta}(\omega, \omega') = (1 - \delta_{z,\beta}) \int d\Omega A_{z,\Omega}^{\text{vac}}(\omega) A_{\beta,\Omega}^{\text{out}}(\omega'), \quad (30)$$

where the Kronecker delta appears for a similar reason as in Eq. (29), implying that  $Q_{ii} = Q_{ss} = 0$ . The second-order correlation function is

$$G_{z\beta\beta z}^{(2)}(\omega, \omega'; \omega', \omega) = G_{zz}^{(1)}(\omega, \omega) G_{\beta\beta}^{(1)}(\omega', \omega') + |G_{z\beta}^{(1)}(\omega, \omega')|^2 + |Q_{z\beta}(\omega, \omega')|^2. \quad (31)$$

Figure 5 presents a schematic chart detailing the simulation procedure employed to calculate the second-order correlation [Eq. (31)]. The simulation involves a fixed pump and crystal configuration that remains constant across all iterations. In each iteration, the initial amplitudes for the signal and idler outputs, denoted as  $A^{\text{out}}$ , are initialized as zero vectors of length  $M$ . Additionally, the vacuum amplitudes,  $A^{\text{vac}}$ , for both signal and idler is set to have a distinct single frequency, represented as a vector of length  $M$  with zeros in all elements except one. The coupled wave equations are then solved using the split-step Fourier method. The resulting solution is utilized to compute the matrices  $G_{z\beta}^{(1)}$  and  $Q_{z\beta}$ , both of size  $M \times M$ . These matrices are updated in each iteration and ultimately summed to derive the second-order correlation matrix  $G_{z\beta\beta z}^{(2)}$ .

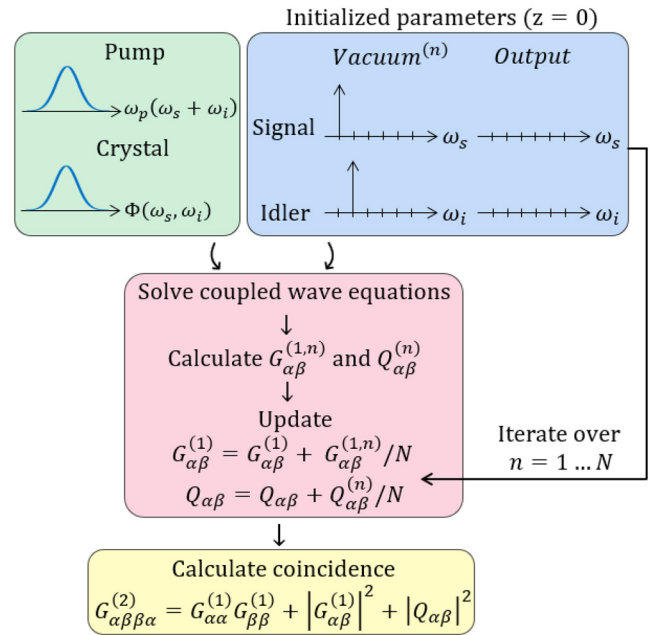


**FIG. 5.** Schematic chart of the simulation procedure. The pump and crystal are determined initially and remain the same for all iterations. In each iteration, the initial signal and idler output wavefunctions  $A^{\text{out}}$  are set to a zero vector of length  $M$ , and the signal and idler vacuum wave function  $A^{\text{vac}}$  are initialized to have a (different) single frequency (a vector of length  $M$  of zeros except one element). The coupled wave equations are then solved using the split-step Fourier method. The output solution is used to calculate  $G_{z\beta}^{(1)}$  and  $Q_{z\beta}$ , which are  $M \times M$  large matrices. In each iteration, these two matrices are updated. Finally, they are summed to calculate the second-order correlation matrix  $G_{z\beta\beta z}^{(2)}$ .

### C. Inverse design

Inverse design in optics draws significant attention these days, enabling the engineering of complex structures ranging from metamaterials to nanophotonics.<sup>71,72</sup> However, its use in nonlinear and quantum optics is still in its infancy. Inverse design of the geometric properties of waveguides was utilized in coherent supercontinuum generation<sup>73</sup> and more recently allowed for the design of reflectors in Fabry–Pérot cavities in silicon carbide for use in quantum and nonlinear optics.<sup>74</sup> Traditionally, nonlinear optics simulation tools rely heavily on the split step method.<sup>54</sup> Therefore, to enjoy the benefits of inverse design in these fields, one may consider incorporating a split-step method into existing optimization algorithms.

One such example of the use of inverse design tools in nonlinear and quantum optics is the SPDCinv inverse design model.<sup>5</sup> This model optimizes (locally) a system's physical parameters to achieve a desired bi-photon state realized through SPDC, using the state's second-order correlation matrix,  $G_{z\beta\beta z}^{(2)}$ , or density matrix as observables. The learning model is physically constrained by the Heisenberg equations of motion and SPDC conservation laws, such that the signal and idler wavelengths and momenta are well-defined. The four coupled Heisenberg equations [Eqs. (23) and (24)] are solved by integrating along the propagation axis using the split-step Fourier method. The model assumes a Gaussian white noise boundary condition at  $z = 0$ , whose standard deviation matches the vacuum field uncertainty, as to not limit the number of supported transverse modes. The vacuum

noise is approximated for all transverse modes by sampling the Gaussian white noise and solving the coupled Heisenberg equation in parallel for the ensemble of realizations.

The SPDCinv model focuses on the physical parameters contained within the interaction coupling coefficients, namely, the crystal's second-order susceptibility and the pump profile. In other words, the model optimizes the pump's transverse profile and the nonlinear crystal's poling profile to achieve the desired bi-photon state. Note that here the propagation is arbitrarily defined along the “z” direction, and the second-order susceptibility is a function of both the transverse location and z. An example in which the model was tasked with designing a nonlinear crystal, which when paired with a Gaussian pump creates the state  $|\psi\rangle = (|1, -2\rangle + |0, -1\rangle + |-1, 0\rangle + |-2, 1\rangle)/\sqrt{4}$  in SPDC, is displayed in Fig. 6. When substituting the Gaussian pump distribution with a Laguerre–Gauss distribution carrying higher-order OAM, the OAM conservation in the resultant biphoton state shifts, demonstrating the dynamic nature of the proposed crystal design. We note that graphics processing units (GPUs) are used for parallel computation and optimization of parameters, unlike simple numerical solutions of the forward models that require regular central processing unit (CPU).

## V. APPLICATIONS OF QUANTUM LIGHT GENERATED BY SHAPED LIGHT AND STRUCTURED CRYSTALS

### A. Spatial domain

A key component of structured light<sup>79</sup> is the spatial degree of freedom, i.e., the phase and amplitude of the electro-magnetic field's

wavefront. The generation of structured quantum optics started in the seminal work by Mair *et al.*<sup>80</sup> There, a shaped pump beam with different topological charges BBO crystal was used to generate entanglement for the down-converted photons between different OAM. Following Eq. (10), many works established the connection between modulated pump beams and the resulting quantum correlations between different spatial modes. For example, Torres *et al.*<sup>81</sup> calculated the “spiral bandwidth”—the relation between the OAM-shaped pump beam and the resulting correlations of the signal and idler with different topological charges. This work was then generalized for the Hermite Gauss basis by Kovlakov *et al.*<sup>82</sup> and Walborn *et al.*<sup>83</sup> Since then, shaping the pump beam in SPDC has been the key method for controlling the entanglement of single photons with different spatial mode profiles. This enabled a plethora of functionalities such as quantum key distribution,<sup>84,85</sup> quantum sensing,<sup>86,87</sup> and quantum computing.<sup>88</sup>

Conversely, using the crystal degree of freedom to control the spatial degree of freedom using modulated nonlinearity has remained scarce until recent years. The first works (see Fig. 7) that took into account the possibility of generating spatial quantum correlations were by Torres *et al.*<sup>89</sup> Then, the first that experimentally showed it is possible to spatially control the emitted photons attributes using nontrivial poling structure were Leng *et al.*<sup>75</sup> Later, nonlinear fork gratings were theoretically proposed for engineering the entanglement between different OAM modes of the down-converted photons.<sup>90,91</sup> The first experimental realization of engineered nonlinear crystals for shaping the quantum correlations were based on two-dimensional periodic

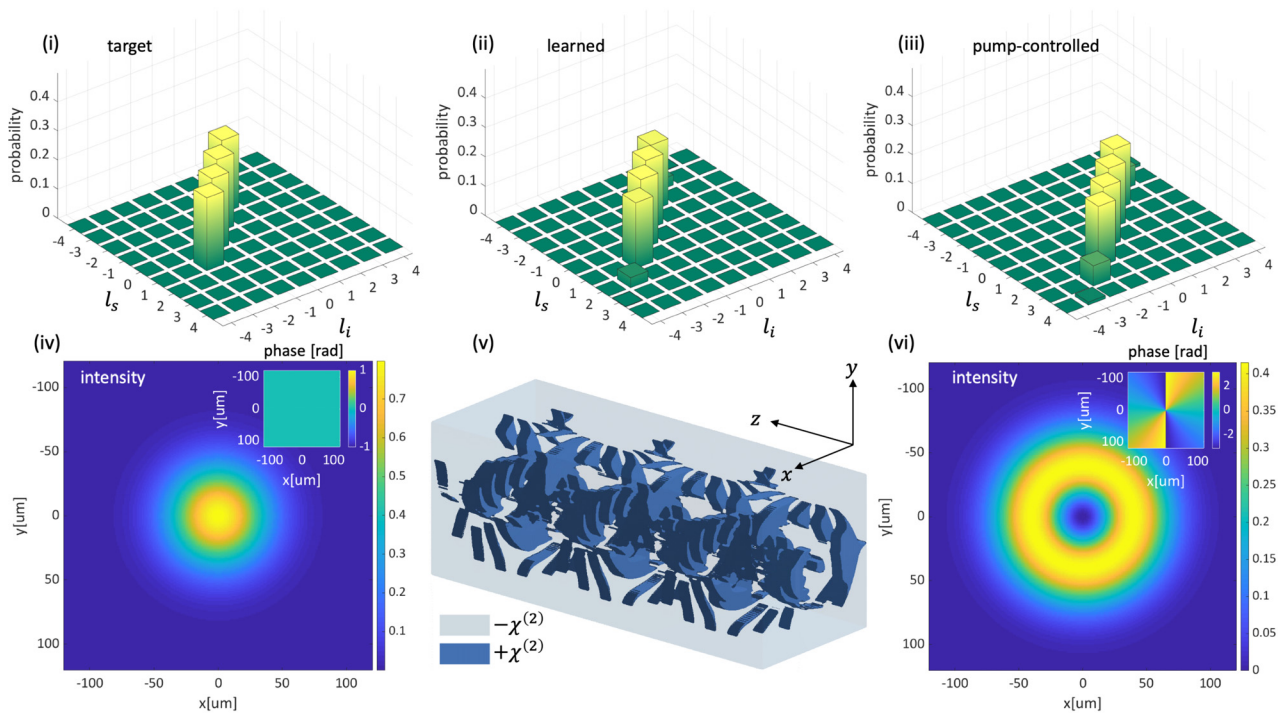


**FIG. 6.** Example of the inverse design of biphoton states.<sup>6</sup> (i) The target observable in the form of signal, idler coincidence counts supplied to the model, and (ii) the learned coincidence counts post-optimization. (iv) and (v) The pump's fixed Gaussian intensity profile, and three unit cells of the locally optimal design of the crystal  $\chi^{(2)}$  parameter. (iii) and (vi) The shifted coincidence counts with higher OAM after changing the Gaussian pump with a  $LG_{0,2}$  pump. Reproduced with permission from Rozenberg *et al.*, *Optica* **9**, 602–615 (2022). Copyright 2022 Optica Publishing Group.<sup>6</sup>



poling, by Megidish *et al.*<sup>92</sup> and Jin *et al.*<sup>93</sup> In these works, the crystal enabled direct generation of path entangled N00N states by engineering the entanglement between different k-vectors of the down-converted photons. More recently, this concept was further extended by Di Domenico *et al.*<sup>76</sup> by using two tilted one-dimensional gratings,

forming a V-shape, see Fig. 7(B). Experiments by Yesharim *et al.*<sup>69</sup> demonstrated how spatial correlations can be shaped using 2D PPKTP crystals, therefore experimentally opening the field of quantum nonlinear holography (QNH). QNH offers several advantages: The most immediate is the miniaturization of the shaping process to the bare

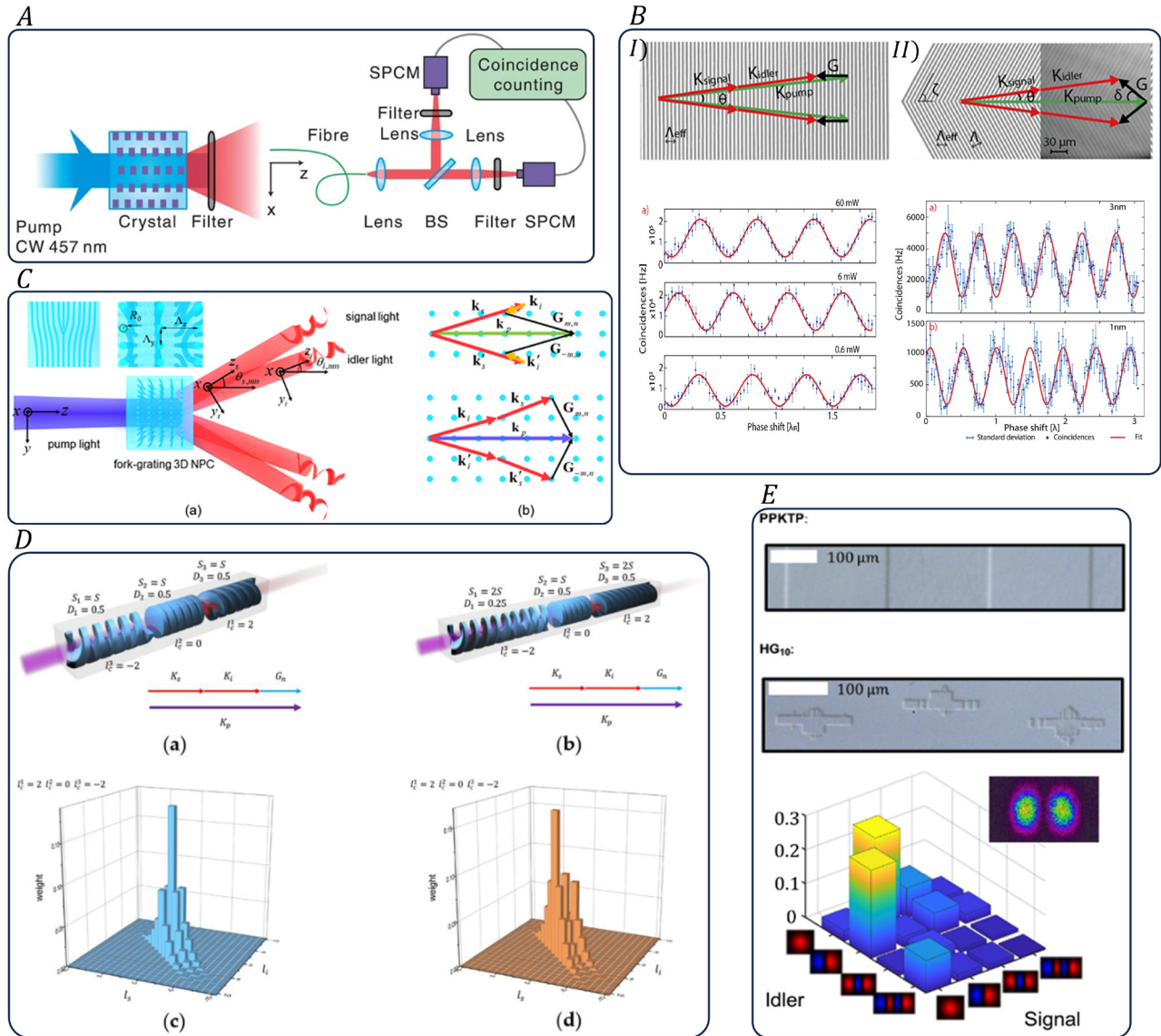


**FIG. 7.** Bulk nonlinear quantum metamaterials in the path and spatial domain. (A) A Gaussian phase for a structured nonlinear crystal (LiNbO<sub>3</sub>) give rise to a focusing effect in SPDC without the need for an extra lens. Reproduced with permission from Leng *et al.*, Nat. Commun. **2**, 429 (2011). Copyright 2021 Springer Nature.<sup>75</sup> (B) Crystal (I) and pump (II) shaping enables direct generation of path-entangled N00N states. Reproduced with permission from Domenico *et al.*, Opt. Express **30**, 21535–21543 (2022). Copyright 2022 Optica Publishing Group.<sup>76</sup> (C) Fork-shaped 3D NLPCs are expected to generate spatial mode entanglement with built-in separation between the signal and idler. Reproduced with permission from Xu *et al.*, Phys. Rev. A **104**, 063716 (2021). Copyright 2021 American Physical Society.<sup>77</sup> (D) Cascaded designs of different spiral quantum nonlinear holograms can engineer different quantum states in a compact manner. Reproduced with permission from Yu *et al.*, Photonics **9**, 504 (2022). Copyright 2022 Authors, licensed under a Creative Commons Attribution (CC BY) license.<sup>78</sup> (E) Experimental results of quantum nonlinear holography. Reproduced with permission from Yesharim *et al.*, Sci. Adv. **9**, eade7968 (2023). Copyright 2023 Authors, licensed under a Creative Commons Attribution (CC BY) license.<sup>69</sup> Microscopic image of the fabricated crystal and its comparison to a standard type-2 PPKP (upper part). Correlations between different spatial modes in the HG basis using the HG<sub>10</sub> NLPC, generating a bell state in the spatial domain (lower part).



minimum, as the crystal already exists in every scheme that uses quadratic nonlinearity for SPDC. However, QNH may potentially be beneficial for ultrafast switching of different quantum states by using different QPM periods on the same crystal.<sup>11,15,16</sup> Recently, with the advent of 3D nonlinear photonic crystals, a new interest became apparent in using the crystal degree of freedom, following three theoretical papers.<sup>6,7,78</sup> Furthermore, using a cascaded design of spatial patterns on the same nonlinear crystal presents an opportunity to overcome challenges in quantum state engineering, stemming for example from the conservation of OAM. In Ref. 94, Kysela *et al.* showed it is possible to shape the spatial quantum correlations by using the path-identity concept. There, three different state generations, resulting from different spatially distributed pump beams, were cascaded to achieve better tunability when compared to a single shaped pump beam. This concept can now be implemented in nonlinear photonic crystals, as theoretically demonstrated by Yu *et al.*<sup>78</sup> In terms of fabrication, QNH still has some challenges for wide usage. For example, the approximate duty cycle (that helps the fabrication process) affects the overall purity of the generated state.<sup>69</sup> In addition, random fabrication errors,<sup>6</sup> changes the target entangled state. This can be partially mitigated by pump shaping, which has its own disadvantages (loss and large footprint).

## B. Spectral domain

In the spectral domain, employing structured crystals enables the creation of Fock states, squeezed quadrature states, and entangled photon pairs, thus paving the way for innovative applications in computing, sensing, and communications.

The manipulation of photon pair spectra via second-order nonlinearity in crystals<sup>95,96,101,102</sup> has emerged as a focal point in photonics research. Illustrated in Fig. 8(A) is an image of a domain-engineered crystal, marking a pioneering effort in utilizing such crystals for generating pure states. A follow-up work [Fig. 8(B)] used simulated annealing to find an optimized poling configuration that allows arbitrary shaping of the PMF, focusing on pure states.

Shaping the PMF enables the creation of high-photon-number multiphoton states, such as heralded Fock states, essential for quantum information processing (QIP). In another study,<sup>98</sup> a method for producing discrete frequency-bin entanglement is introduced, distinct from conventional techniques involving filtering or resonant cavities. This approach employs a domain-engineered nonlinear crystal to create an eight-mode frequency-bin entangled source operating at telecommunication wavelengths [Fig. 8(C)]. The method capitalizes on the advantages of bulk crystal sources, including high heralding efficiency and straightforward implementation.

Moreover, a combined approach demonstrating two-dimensional control JSI has been shown.<sup>99</sup> This method involves controlling two degrees of freedom: the phase-matching function and the pump spectrum. Such control enables the experimental generation of a diverse range of spectrally encoded quantum states, including frequency uncorrelated states, frequency-bin Bell states, biphoton qudit states, as well as a four-lobe state [Fig. 8(D)]. Additionally, theoretical analyses have indicated the feasibility of generating a square cluster state using this method.<sup>63</sup>

In another study,<sup>50</sup> researchers manipulate the dispersion and quasi-phase-matching conditions of a waveguide in thin-film lithium niobate to generate spectrally separable photon pairs in the

telecommunications band. As depicted in Fig. 8(E), the figure illustrates a deleted-domain Gaussian-apodized poling electrode pattern and a two-photon microscopy image of the poled film on the right, alongside a JSI measured using dispersion-engineered thin-film lithium niobate on the left. This design leverages waveguide geometry-induced dispersion to fulfill the group velocity matching (GVM) condition, enabling the generation of a spectrally separable biphoton state.

Domain-engineered NLPCs offer a pathway to simplify the generation of frequency combs. Some studies employ periodically poled NLPCs within complex configurations to produce desired entangled states. Figure 8(F) illustrates the concept of entanglement within a quantum optical frequency comb. In a sophisticated experimental arrangement,<sup>100</sup> two periodically poled KTPs are employed to create and characterize a dual-rail quantum-wire cluster state within the quantum optical frequency comb. Another experiment<sup>103</sup> utilizes periodically poled lithium niobate to establish frequency bins. Incorporating domain-engineered NLPCs has the potential to enhance robustness and streamline experimental setups.

## C. Hyperentanglement

In recent years, the exploration of hyperentanglement,<sup>104</sup> defined as the combination of two or more degrees of freedom (DOFs) of light, has gained significant attention in quantum optics. Hyperentanglement presents an avenue for expanding the Hilbert space. Such a set of entangled states not only facilitates selective control and measurements of individual subsystems but also holds the potential to enhance existing quantum protocols and introduce novel ones.

The first experimental validation of hyperentanglement across all DOFs<sup>105</sup> employed photon pairs generated in SPDC. Entanglement was confirmed by observing a Bell-type inequality violation in polarization, spatial mode, and time energy. The distinctive feature of hyperentanglement, as explored in the literature, is its ability to enable advanced quantum protocols, such as complete Bell-state analysis.<sup>106,107</sup> Notably, it has played a pivotal role in achieving the teleportation of multiple DOFs of a single photon.<sup>108</sup>

A manifestation of hyperentanglement involving spectrum, polarization, and OAM DOFs was successfully demonstrated.<sup>109</sup> By encoding entanglement between these photons' properties, the research not only expands information capacities but also promises the development of quantum protocols. Notably, these hyperentangled states exhibit a more intricate entanglement structure compared to previous demonstrations, owing to their incorporation of both the spectral and spatial characteristics of light.

Overall, this research provides a robust method for generating high-dimensional entanglement in photon pairs, paving the way for exciting applications in quantum communication, cryptography, and computation.

## VI. SUMMARY AND OUTLOOK

To summarize, bulk nonlinear quantum metamaterials are now seeing an experimental and theoretical surge, thanks to advantages of simplicity, compact size, robustness, enhanced control over generated quantum states, and power efficiency. We expect that this is merely the beginning of a vibrant field that will evolve rapidly due to the need for sophisticated quantum light sources and owing to improvement of fabrication technologies such as 3D NLPC using fs lasers and electric field poling in both waveguide and bulk configurations. One of the

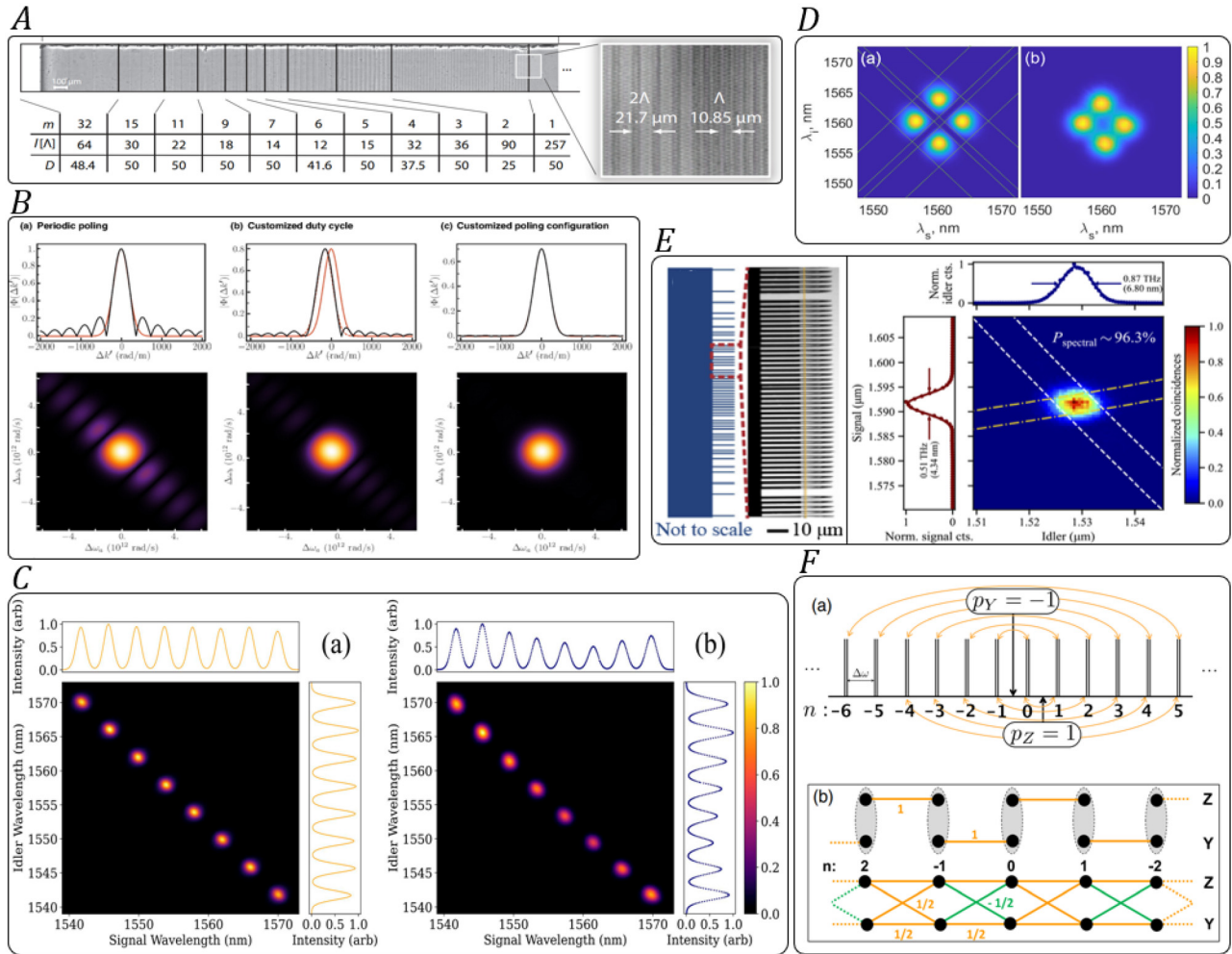


**FIG. 8.** Applications in the spectral domain. (A) Image of a custom-poled KTP crystal with an approximately Gaussian nonlinearity profile. Reproduced with permission from Opt. Express **19**, 55–65 (2011). Copyright 2011 Optica Publishing Group.<sup>95</sup> (B) Comparison of phase-matching functions (top), joint spectral amplitudes (bottom) for different apodization schemes. Reproduced with permission from Dosseva *et al.*, Phys. Rev. A **93**, 013801 (2016). Copyright 2016 American Physical Society.<sup>96</sup> (a) Standard first-order periodically poled crystal (no apodization). (b) Customized duty cycle method.<sup>97</sup> (c) Custom-poled crystal generated using simulated annealing. (C) Theoretical (a) and experimentally measured (b) joint spectral intensity using domain-engineered crystal. Reproduced from Morrison *et al.*, APL Photonics **7**, 066102 (2022) with the permission of AIP Publishing.<sup>98</sup> (D) JSI from a double-lobe domain-engineered crystal with a modulated pump spectrum: (a) simulated and (b) experimentally measured. Reproduced with permission from Shukhin *et al.*, Opt. Express **32**, 10158–10174 (2024). Copyright 2024 Optica Publishing Group.<sup>99</sup> (E) Deleted-domain Gaussian-apodized poling electrode pattern and two-photon microscopy image of the poled film (right). JSI measured using dispersion-engineered thin-film lithium niobate (left). Reproduced with permission from Xin *et al.*, Opt. Lett. **47**, 2830–2833 (2022). Copyright 2022 Optica Publishing Group.<sup>50</sup> (F) Generation of a dual-rail quantum wire in the quantum optical frequency comb. Reproduced with permission from Graffitti *et al.*, Phys. Rev. Lett. **112**, 120505 (2014). Copyright 2014 American Physical Society.<sup>100</sup> (a) EPR pairs are created by interactions in the quantum optical frequency comb of a polarization-degenerate OPO. (b) Quantum graph states. The initial EPR pairs from the OPO (top) turn into a dual-rail CV cluster state (bottom).

next important tasks is to integrate these crystals into existing quantum information processing (QIP) schemes to leverage their advantages. We believe that this will indeed be the case, as regular periodically poled crystals already exist in many QIP experimental schemes. The design and fabrication of bulk quantum metamaterials is the major hurdle in wide adoption of the aforementioned advantages.

One such task is integrating quantum error-correcting capabilities into computation, communication, and information-processing

hardware. In contrast to classical bits of information, quantum bits cannot be protected against error using repetition code due to the no-cloning theorem.

The solution of encoding the logical quantum bits into highly entangled physical quantum states was theorized by Peter Shor and demonstrated for nine entangled qubits.<sup>110</sup> The materialization of Cat, GKP, and cluster state theory created another avenue of error detection, analysis, and correction in QIP schemes. The prospect of creating

Cat and cluster states through photon–metasurface interactions was demonstrated in Ref. 111, providing a potential method for on-chip integration of error-correction capabilities in such QIP schemes.

Additional advances can be made in QIP by utilizing the combination of inverse design methods and emerging 3D poling techniques to achieve high-dimensional and optically controlled quantum states, as demonstrated in Fig. 6. Integrating high-frequency modulators into such optical designs could breed a new practical method processing of light signals.

## AUTHOR DECLARATIONS

### Conflict of Interest

The authors have no conflicts to disclose.

### Author Contributions

O. Yesharim and I. Hurvitz contributed equally to this work.

**Ofir Yesharim:** Methodology (equal); Writing – original draft (equal); Writing – review & editing (equal). **Inbar Hurvitz:** Methodology (equal); Writing – original draft (equal); Writing – review & editing (equal). **Joshua Foley-Comer:** Methodology (equal); Writing – original draft (equal); Writing – review & editing (equal). **Ady Arie:** Conceptualization (equal); Funding acquisition (equal); Supervision (equal); Writing – original draft (equal); Writing – review & editing (equal).

### DATA AVAILABILITY

The data that support the findings of this study are available from the corresponding author upon reasonable request.

## REFERENCES

- M. A. Nielsen and I. L. Chuang, *Quantum Computation and Quantum Information: 10th Anniversary Edition* (Cambridge University Press, 2010).
- P. G. Kwiat, K. Mattle, H. Weinfurter, and A. Zeilinger, “New high-intensity source of polarization-entangled photon pairs,” *Phys. Rev. Lett.* **75**, 4337–4341 (1995).
- N. J. Cerf, M. Bourennane, A. Karlsson, and N. Gisin, “Security of quantum key distribution using  $d$ -level systems,” *Phys. Rev. Lett.* **88**, 127902 (2002).
- D. Bruß and C. Macchiavello, “Optimal eavesdropping in cryptography with three-dimensional quantum states,” *Phys. Rev. Lett.* **88**, 127901 (2002).
- S. Trajtenberg-Mills, A. Karnieli, N. Voloch-Bloch, E. Megidish, H. S. Eisenberg, and A. Arie, “Simulating correlations of structured spontaneously down-converted photon pairs,” *Laser Photonics Rev.* **14**, 1900321 (2020).
- E. Rozenberg, A. Karnieli, O. Yesharim, J. Foley-Comer, S. Trajtenberg-Mills, D. Freedman, A. M. Bronstein, and A. Arie, “Inverse design of spontaneous parametric downconversion for generation of high-dimensional qudits,” *Optica* **9**, 602–615 (2022a).
- D. Wei, C. Wang, H. Wang, X. Hu, D. Wei, X. Fang, Y. Zhang, D. Wu, Y. Hu, J. Li, S. Zhu, and M. Xiao, “Experimental demonstration of a three dimensional lithium niobate nonlinear photonic crystal,” *Nat. Photonics* **12**, 596–600 (2018).
- T. Xu, K. Switkowski, X. Chen, S. Liu, K. Koynov, H. Yu, H. Zhang, J. Wang, Y. Sheng, and W. Krolikowski, “Three-dimensional nonlinear photonic crystal in ferroelectric barium calcium titanate,” *Nat. Photonics* **12**, 591–595 (2018).
- Y. Zhang, Y. Sheng, S. Zhu, M. Xiao, and W. Krolikowski, “Nonlinear photonic crystals: From 2D to 3D,” *Optica* **8**, 372–381 (2021).
- S. Trajtenberg-Mills and A. Arie, “Shaping light beams in nonlinear processes using structured light and patterned crystals,” *Opt. Mater. Express* **7**, 2928–2942 (2017).
- T. Ellenbogen, N. Voloch-Bloch, A. Ganany-Padowicz, and A. Arie, “Nonlinear generation and manipulation of airy beams,” *Nat. Photonics* **3**, 395–398 (2009).
- N. V. Bloch, K. Shemer, A. Shapira, R. Shiloh, I. Juviler, and A. Arie, “Twisting light by nonlinear photonic crystals,” *Phys. Rev. Lett.* **108**, 233902 (2012).
- D. Wei, C. Wang, X. Xu, H. Wang, Y. Hu, P. Chen, J. Li, Y. Zhu, C. Xin, X. Hu, Y. Zhang, D. Wu, J. Chu, S. Zhu, and M. Xiao, “Efficient nonlinear beam shaping in three-dimensional lithium niobate nonlinear photonic crystals,” *Nat. Commun.* **10**, 4193 (2019).
- S. Liu, K. Switkowski, C. Xu, J. Tian, B. Wang, P. Lu, W. Krolikowski, and Y. Sheng, “Nonlinear wavefront shaping with optically induced three-dimensional nonlinear photonic crystals,” *Nat. Commun.* **10**, 3208 (2019).
- P. Chen, C. Wang, D. Wei, Y. Hu, X. Xu, J. Li, D. Wu, J. Ma, S. Ji, L. Zhang, L. Xu, T. Wang, C. Xu, J. Chu, S. Zhu, M. Xiao, and Y. Zhang, “Quasi-phase-matching-division multiplexing holography in a three-dimensional nonlinear photonic crystal,” *Light: Sci. Appl.* **10**, 146 (2021).
- A. Arie, “Storing and retrieving multiple images in 3D nonlinear photonic crystals,” *Light: Sci. Appl.* **10**, 202 (2021).
- R. Shiloh and A. Arie, “Spectral and temporal holograms with nonlinear optics,” *Opt. Lett.* **37**, 3591–3593 (2012).
- A. Leshem, R. Shiloh, and A. Arie, “Experimental realization of spectral shaping using nonlinear optical holograms,” *Opt. Lett.* **39**, 5370–5373 (2014).
- A. Anwar, C. Perumangatt, F. Steinlechner, T. Jennewein, and A. Ling, “Entangled photon-pair sources based on three-wave mixing in bulk crystals,” *Rev. Sci. Instrum.* **92**, 041101 (2021).
- J. P. Torres, K. Banaszek, and I. A. Walmsley, “Engineering nonlinear optical sources of photonic entanglement,” in *Progress in Optics*, edited by E. Wolf (Elsevier, 2011), Vol. 56, Chap. 5, pp. 227–331.
- R. W. Boyd, *Nonlinear Optics*, 3rd ed. (Academic Press, Inc., USA, 2008).
- C. T. Lee, “Nonclassical photon statistics of two-mode squeezed states,” *Phys. Rev. A* **42**, 1608–1616 (1990).
- J. A. Armstrong, N. Bloembergen, J. Ducuing, and P. S. Pershan, “Interactions between light waves in a nonlinear dielectric,” *Phys. Rev.* **127**, 1918–1939 (1962).
- V. Berger, “Nonlinear photonic crystals,” *Phys. Rev. Lett.* **81**, 4136–4139 (1998).
- N. G. R. Broderick, G. W. Ross, H. L. Offerhaus, D. J. Richardson, and D. C. Hanna, “Hexagonally poled lithium niobate: A two-dimensional nonlinear photonic crystal,” *Phys. Rev. Lett.* **84**, 4345–4348 (2000).
- N. H. A. Arie and A. Bahabad, “Quasi phase matching in two-dimensional nonlinear photonic crystals,” *Opt. Quantum Electron.* **39**, 361–375 (2007).
- S. N. Zhu, Y. Y. Zhu, and N. B. Ming, “Quasi-phase-matched third-harmonic generation in a quasi-periodic optical superlattice,” *Science* **278**, 843–846 (1997).
- R. Lifshitz, A. Arie, and A. Bahabad, “Photonic quasicrystals for nonlinear optical frequency conversion,” *Phys. Rev. Lett.* **95**, 133901 (2005).
- A. Arie and N. Voloch, “Periodic, quasi-periodic, and random quadratic nonlinear photonic crystals,” *Laser Photonics Rev.* **4**, 355–373 (2010).
- H. Suchowski, D. Oron, A. Arie, and Y. Silberberg, “Geometrical representation of sum frequency generation and adiabatic frequency conversion,” *Phys. Rev. A* **78**, 063821 (2008).
- H. Suchowski, G. Porat, and A. Arie, “Adiabatic processes in frequency conversion,” *Laser Photonics Rev.* **8**, 333–367 (2014).
- M. Houe and P. D. Townsend, “An introduction to methods of periodic poling for second-harmonic generation,” *J. Phys. D: Appl. Phys.* **28**, 1747 (1995).
- Y. Glickman, E. Winebrand, A. Arie, and G. Rosenman, “Electron-beam-induced domain poling in LiNbO<sub>3</sub> for two-dimensional nonlinear frequency conversion,” *Appl. Phys. Lett.* **88**, 011103 (2006).
- X. Chen, P. Karpinski, V. Shvedov, A. Boes, A. Mitchell, W. Krolikowski, and Y. Sheng, “Quasi-phase matching via femtosecond laser-induced domain inversion in lithium niobate waveguides,” *Opt. Lett.* **41**, 2410–2413 (2016).
- M. Yamada, N. Nada, M. Saitoh, and K. Watanabe, “First-order quasi-phase matched LiNbO<sub>3</sub> waveguide periodically poled by applying an external field for efficient blue second-harmonic generation,” *Appl. Phys. Lett.* **62**, 435–436 (1993).
- H. Ishizuki and T. Taira, “Half-joule output optical-parametric oscillation by using 10-mm-thick periodically poled mg-doped congruent LiNbO<sub>3</sub>,” *Opt. Express* **20**, 20002–20010 (2012).



- <sup>37</sup>P. Mutter, K. M. Molster, A. Zukauskas, V. Pasiskevicius, and C. Canalias, "Efficient first-order quasi-phase-matched backward second-harmonic generation," *Opt. Lett.* **48**, 1534–1537 (2023).
- <sup>38</sup>X. Xu, T. Wang, P. Chen, C. Zhou, J. Ma, D. Wei, H. Wang, B. Niu, X. Fang, D. Wu, S. Zhu, M. Gu, M. Xiao, and Y. Zhang, "Femtosecond laser writing of lithium niobate ferroelectric nanodomains," *Nature* **609**, 496–501 (2022).
- <sup>39</sup>S. Liu, L. Wang, L. M. Mazur, K. Switkowski, B. Wang, F. Chen, A. Arie, W. Krolkowski, and Y. Sheng, "Highly efficient 3D nonlinear photonic crystals in ferroelectrics," *Adv. Opt. Mater.* **11**, 2300021 (2023).
- <sup>40</sup>A. Boes, L. Chang, C. Langrock, M. Yu, M. Zhang, Q. Lin, M. Lončar, M. Fejer, J. Bowers, and A. Mitchell, "Lithium niobate photonics: Unlocking the electromagnetic spectrum," *Science* **379**, eabj4396 (2023).
- <sup>41</sup>J. Gil-Lopez, M. Santandrea, G. Roeland, B. Brecht, C. Eigner, R. Ricken, V. Quiring, and C. Silberhorn, "Improved non-linear devices for quantum applications," *New J. Phys.* **23**, 063082 (2021).
- <sup>42</sup>M. M. Fejer, "Thin-film lithium niobate waveguides for quantum photonics," *Proc. SPIE* **12911**, 129110A (2024).
- <sup>43</sup>R. V. Schmidt and I. P. Kaminow, "Metal-diffused optical waveguides in LiNbO<sub>3</sub>," *Appl. Phys. Lett.* **25**, 458–460 (1974).
- <sup>44</sup>J. L. Jackel, C. E. Rice, and J. J. Veselka, "Proton exchange for high-index waveguides in LiNbO<sub>3</sub>," *Appl. Phys. Lett.* **41**, 607–608 (1982).
- <sup>45</sup>F. Laurell, M. G. Roelofs, W. Bindloss, H. Hsiung, A. Suna, and J. D. Bierlein, "Detection of ferroelectric domain reversal in KTiOPO<sub>4</sub> waveguides," *J. Appl. Phys.* **71**, 4664–4670 (1992).
- <sup>46</sup>D. Eger, M. Oron, M. Katz, and A. Zussman, "Highly efficient blue light generation in KTiOPO<sub>4</sub> waveguides," *Appl. Phys. Lett.* **64**, 3208–3209 (1994).
- <sup>47</sup>D. Zhu, L. Shao, M. Yu, R. Cheng, B. Desiatov, C. J. Xin, Y. Hu, J. Holzgrafe, S. Ghosh, A. Shams-Ansari, E. Puma, N. Sinclair, C. Reimer, M. Zhang, and M. Lončar, "Integrated photonics on thin-film lithium niobate," *Adv. Opt. Photonics* **13**, 242–352 (2021).
- <sup>48</sup>D. S. Hum and M. M. Fejer, "Quasi-phases matching," *C. R. Phys.* **8**, 180–198 (2007).
- <sup>49</sup>B. E. A. Saleh and M. C. Teich, "Guided-wave optics," in *Fundamentals of Photonics* (John Wiley & Sons, Ltd, 1991), Chap. 7, pp. 238–271.
- <sup>50</sup>C. J. Xin, J. N. Mishra, C. Chen, D. Zhu, A. Shams-Ansari, C. Langrock, N. Sinclair, F. N. C. Wong, M. M. Fejer, and M. Lončar, "Spectrally separable photon-pair generation in dispersion engineered thin-film lithium niobate," *Opt. Lett.* **47**, 2830–2833 (2022).
- <sup>51</sup>Z. Zheng, D. Rocco, H. Ren, O. Sergaeva, Y. Zhang, K. B. Whaley, C. Ying, D. de Ceglia, C. De-Angelis, M. Rahmani, and L. Xu, "Advances in nonlinear metasurfaces for imaging, quantum, and sensing applications," *Nanophotonics* **12**, 4255–4281 (2023).
- <sup>52</sup>T. Santiago-Cruz, S. D. Gennaro, O. Mitrofanov, S. Addamane, J. Reno, I. Brener, and M. V. Chekhova, "Resonant metasurfaces for generating complex quantum states," *Science* **377**, 991–995 (2022).
- <sup>53</sup>J. Zhang, J. Ma, M. Parry, M. Cai, R. Camacho-Morales, L. Xu, D. N. Neshev, and A. A. Sukhorukov, "Spatially entangled photon pairs from lithium niobate nonlocal metasurfaces," *Sci. Adv.* **8**, eabq4240 (2022).
- <sup>54</sup>B. Jin, D. Mishra, and C. Argyropoulos, "Efficient single-photon pair generation by spontaneous parametric down-conversion in nonlinear plasmonic metasurfaces," *Nanoscale* **13**, 19903–19914 (2021).
- <sup>55</sup>Y. S. Tokpanov, J. S. Fakonas, B. Vest, and H. A. Atwater, "Quantum coherence preservation in extremely dispersive plasmonic media," *Phys. Rev. Appl.* **12**, 044037 (2019).
- <sup>56</sup>A. S. Solntsev, G. S. Agarwal, and Y. S. Kivshar, "Metasurfaces for quantum photonics," *Nat. Photonics* **15**, 327–336 (2021).
- <sup>57</sup>K. Wang, M. Chekhova, and Y. Kivshar, "Metasurfaces for quantum technologies," *Phys. Today* **75**(8), 38–44 (2022).
- <sup>58</sup>E. Nagali, F. Sciarrino, F. De Martini, L. Marrucci, B. Piccirillo, E. Karimi, and E. Santamato, "Quantum information transfer from spin to orbital angular momentum of photons," *Phys. Rev. Lett.* **103**, 013601 (2009).
- <sup>59</sup>T. Stav, A. Faerman, E. Maguid, D. Oren, V. Kleiner, E. Hasman, and M. Segev, "Quantum entanglement of the spin and orbital angular momentum of photons using metamaterials," *Science* **361**, 1101–1104 (2018).
- <sup>60</sup>G. Kulkarni, J. Rioux, B. Braverman, M. V. Chekhova, and R. W. Boyd, "Classical model of spontaneous parametric down-conversion," *Phys. Rev. Res.* **4**, 033098 (2022).
- <sup>61</sup>See the supplementary material for Ref. 6, "Supplementary document for inverse design of spontaneous parametric down conversion for generation of high-dimensional qudits."
- <sup>62</sup>J. C. Garrison and R. Y. Chiao, *Quantum Optics* (Oxford University, 2008).
- <sup>63</sup>I. Hurvitz, A. Karnieli, and A. Arie, "Frequency-domain engineering of bright squeezed vacuum for continuous-variable quantum information," *Opt. Express* **31**, 20387–20397 (2023).
- <sup>64</sup>G. Agrawal, *Nonlinear Fibre Optics*, 4th ed. (Academic Press, 2007).
- <sup>65</sup>E. Brambilla, A. Gatti, M. Bache, and L. A. Lugiato, "Simultaneous near-field and far-field spatial quantum correlations in the high-gain regime of parametric down-conversion," *Phys. Rev. A* **69**, 023802 (2004).
- <sup>66</sup>V. D. Salakhutdinov, E. R. Eliel, and W. Löffler, "Full-field quantum correlations of spatially entangled photons," *Phys. Rev. Lett.* **108**, 173604 (2012).
- <sup>67</sup>M. Malik, M. Erhard, M. Huber, M. Krenn, R. Fickler, and A. Zeilinger, "Multi-photon entanglement in high dimensions," *Nat. Photonics* **10**, 248–252 (2016).
- <sup>68</sup>R. Fickler, R. Lapkiewicz, W. N. Plick, M. Krenn, C. Schaeff, S. Ramelow, and A. Zeilinger, "Quantum entanglement of high angular momenta," *Science* **338**, 640–643 (2012).
- <sup>69</sup>O. Yesharim, S. Pearl, J. Foley-Comer, I. Juwiler, and A. Arie, "Direct generation of spatially entangled qudits using quantum nonlinear optical holography," *Sci. Adv.* **9**, eade7968 (2023).
- <sup>70</sup>F. Graffitti, P. Barrow, A. Pickston, A. M. Brańczyk, and A. Fedrizzi, "Direct generation of tailored pulse-mode entanglement," *Phys. Rev. Lett.* **124**, 053603 (2020a).
- <sup>71</sup>S. Molesky, Z. Lin, A. Piggott, W. Jin, J. Vučković, and A. Rodriguez, "Inverse design in nanophotonics," *Nat. Photonics* **12**, 659–670 (2018).
- <sup>72</sup>S. So, T. Badloe, J. Noh, J. Bravo-Abad, and J. Rho, "Deep learning enabled inverse design in nanophotonics," *Nanophotonics* **9**, 1041–1057 (2020).
- <sup>73</sup>C.-Y. Lee, Y. Liu, Y. Cheng, C. Lao, and Q.-F. Yang, "Inverse design of coherent supercontinuum generation using free-form nanophotonic waveguides," *APL Photonics* **9**, 066108 (2024).
- <sup>74</sup>J. Yang, M. A. Guidry, D. M. Lukin, K. Yang, and J. Vučković, "Inverse-designed silicon carbide quantum and nonlinear photonics," *Light: Sci. Appl.* **12**, 201 (2023).
- <sup>75</sup>H. Y. Leng, X. Q. Yu, Y. X. Gong, P. Xu, Z. D. Xie, H. Jin, C. Zhang, and S. N. Zhu, "On-chip steering of entangled photons in nonlinear photonic crystals," *Nat. Commun.* **2**, 429 (2011).
- <sup>76</sup>G. D. Domenico, S. Pearl, A. Karnieli, S. Trajtenberg-Mills, I. Juwiler, H. S. Eisenberg, and A. Arie, "Direct generation of high brightness path entangled N00N states using structured crystals and shaped pump beams," *Opt. Express* **30**, 21535–21543 (2022).
- <sup>77</sup>C. Xu, S. Huang, Q. Yu, D. Wei, P. Chen, S. Nie, Y. Zhang, and M. Xiao, "Manipulating the orbital-angular-momentum correlation of entangled two-photon states in three-dimensional nonlinear photonic crystals," *Phys. Rev. A* **104**, 063716 (2021).
- <sup>78</sup>Q. Yu, C. Xu, S. Chen, P. Chen, S. Nie, S. Ke, D. Wei, M. Xiao, and Y. Zhang, "Manipulating orbital angular momentum entanglement in three-dimensional spiral nonlinear photonic crystals," *Photonics* **9**, 504 (2022).
- <sup>79</sup>H. Rubinsztein-Dunlop, A. Forbes, M. V. Berry, M. R. Dennis, D. L. Andrews, M. Mansuripur, C. Denz, C. Alpmann, P. Banzer, T. Bauer, E. Karimi, L. Marrucci, M. Padgett, M. Ritsch-Marte, N. M. Litchinitser, N. P. Bigelow, C. Rosales-Guzmán, A. Belmonte, J. P. Torres, T. W. Neely, M. Baker, R. Gordon, A. B. Stilgoe, J. Romero, A. G. White, R. Fickler, A. E. Willner, G. Xie, B. McMorrin, and A. M. Weiner, "Roadmap on structured light," *J. Opt.* **19**, 013001 (2017).
- <sup>80</sup>A. Mair, A. Vaziri, G. Weihs, and A. Zeilinger, "Entanglement of the orbital angular momentum states of photons," *Nature* **412**, 313–316 (2001).
- <sup>81</sup>J. P. Torres, A. Alexandrescu, and L. Torner, "Quantum spiral bandwidth of entangled two-photon states," *Phys. Rev. A* **68**, 050301 (2003).
- <sup>82</sup>E. V. Kovalkov, I. B. Bobrov, S. S. Straupe, and S. P. Kulik, "Spatial bell-state generation without transverse mode subspace postselection," *Phys. Rev. Lett.* **118**, 030503 (2017).
- <sup>83</sup>S. P. Walborn, S. Pádua, and C. H. Monken, "Conservation and entanglement of Hermite–Gaussian modes in parametric down-conversion," *Phys. Rev. A* **71**, 053812 (2005).



- <sup>84</sup>A. Sit, F. Bouchard, R. Fickler, J. Gagnon-Bischoff, H. Larocque, K. Heshami, D. Elser, C. Peuntinger, K. Günthner, B. Heim, C. Marquardt, G. Leuchs, R. W. Boyd, and E. Karimi, “High-dimensional intracity quantum cryptography with structured photons,” *Optica* **4**, 1006–1010 (2017).
- <sup>85</sup>M. Erhard, R. Fickler, M. Krenn, and A. Zeilinger, “Twisted photons: New quantum perspectives in high dimensions,” *Light: Sci. Appl.* **7**, 17146–17146 (2017).
- <sup>86</sup>M. Hiekkamäki, F. Bouchard, and R. Fickler, “Photonic angular superresolution using twisted N00N states,” *Phys. Rev. Lett.* **127**, 263601 (2021).
- <sup>87</sup>A. K. Jha, G. S. Agarwal, and R. W. Boyd, “Supersensitive measurement of angular displacements using entangled photons,” *Phys. Rev. A* **83**, 053829 (2011).
- <sup>88</sup>F. Brandt, M. Hiekkamäki, F. Bouchard, M. Huber, and R. Fickler, “High-dimensional quantum gates using full-field spatial modes of photons,” *Optica* **7**, 98–107 (2020).
- <sup>89</sup>J. P. Torres, A. Alexandrescu, S. Carrasco, and L. Torner, “Quasi-phase-matching engineering for spatial control of entangled two-photon states,” *Opt. Lett.* **29**, 376–378 (2004).
- <sup>90</sup>Y. Ming, J. Tang, Z.-X. Chen, F. Xu, L.-J. Zhang, and Y.-Q. Lu, “Generation of N00N state with orbital angular momentum in a twisted nonlinear photonic crystal,” *IEEE J. Sel. Top. Quantum Electron.* **21**, 225–230 (2015).
- <sup>91</sup>L. L. Lu, P. Xu, M. L. Zhong, Y. F. Bai, and S. N. Zhu, “Orbital angular momentum entanglement via fork-poling nonlinear photonic crystals,” *Opt. Express* **23**, 1203–1212 (2015).
- <sup>92</sup>E. Megjidiš, A. Halevy, H. S. Eisenberg, A. Ganany-Padowicz, N. Habshoosh, and A. Arie, “Compact 2D nonlinear photonic crystal source of beamlike path entangled photons,” *Opt. Express* **21**, 6689–6696 (2013).
- <sup>93</sup>H. Jin, P. Xu, X. W. Luo, H. Y. Leng, Y. X. Gong, W. J. Yu, M. L. Zhong, G. Zhao, and S. N. Zhu, “Compact engineering of path-entangled sources from a monolithic quadratic nonlinear photonic crystal,” *Phys. Rev. Lett.* **111**, 023603 (2013).
- <sup>94</sup>J. Kysela, M. Erhard, A. Hochrainer, M. Krenn, and A. Zeilinger, “Path identity as a source of high-dimensional entanglement,” *Proc. Natl. Acad. Sci. U. S. A.* **117**, 26118–26122 (2020).
- <sup>95</sup>A. M. Brańczyk, A. Fedrizzi, T. M. Stace, T. C. Ralph, and A. G. White, “Engineered optical nonlinearity for quantum light sources,” *Opt. Express* **19**, 55–65 (2011).
- <sup>96</sup>A. Dosseva, L. Cincio, and A. M. Brańczyk, “Shaping the joint spectrum of down-converted photons through optimized custom poling,” *Phys. Rev. A* **93**, 013801 (2016).
- <sup>97</sup>P. B. Dixon, J. H. Shapiro, and F. N. C. Wong, “Spectral engineering by gaussian phase-matching for quantum photonics,” *Opt. Express* **21**, 5879–5890 (2013).
- <sup>98</sup>C. L. Morrison, F. Graffitti, P. Barrow, A. Pickston, J. Ho, and A. Fedrizzi, “Frequency-bin entanglement from domain-engineered down-conversion,” *APL Photonics* **7**, 066102 (2022).
- <sup>99</sup>A. Shukhin, I. Hurvitz, S. Trajtenberg-Mills, A. Arie, and H. Eisenberg, “Two-dimensional control of a biphoton joint spectrum,” *Opt. Express* **32**, 10158–10174 (2024).
- <sup>100</sup>M. Chen, N. C. Menicucci, and O. Pfister, “Experimental realization of multipartite entanglement of 60 modes of a quantum optical frequency comb,” *Phys. Rev. Lett.* **112**, 120505 (2014).
- <sup>101</sup>F. Graffitti, D. Kundys, D. T. Reid, A. M. Brańczyk, and A. Fedrizzi, “Pure down-conversion photons through sub-coherence-length domain engineering,” *Quantum Sci. Technol.* **2**, 035001 (2017).
- <sup>102</sup>F. Graffitti, P. Barrow, M. Proietti, D. Kundys, and A. Fedrizzi, “Independent high-purity photons created in domain-engineered crystals,” *Optica* **5**, 514–517 (2018).
- <sup>103</sup>H.-H. Lu, J. M. Lukens, N. A. Peters, B. P. Williams, A. M. Weiner, and P. Lougovski, “Quantum interference and correlation control of frequency-bin qubits,” *Optica* **5**, 1455–1460 (2018).
- <sup>104</sup>P. G. Kwiat, “Hyper-entangled states,” *J. Mod. Opt.* **44**, 2173–2184 (1997).
- <sup>105</sup>J. T. Barreiro, N. K. Langford, N. A. Peters, and P. G. Kwiat, “Generation of hyperentangled photon pairs,” *Phys. Rev. Lett.* **95**, 260501 (2005).
- <sup>106</sup>S. P. Walborn, S. Pádua, and C. H. Monken, “Hyperentanglement-assisted bell-state analysis,” *Phys. Rev. A* **68**, 042313 (2003).
- <sup>107</sup>C. Schuck, G. Huber, C. Kurtsiefer, and H. Weinfurter, “Complete deterministic linear optics bell state analysis,” *Phys. Rev. Lett.* **96**, 190501 (2006).
- <sup>108</sup>X.-L. Wang, X.-D. Cai, Z.-E. Su, M.-C. Chen, D. Wu, L. Li, N.-L. Liu, C.-Y. Lu, and J.-W. Pan, “Quantum teleportation of multiple degrees of freedom of a single photon,” *Nature* **518**, 516–519 (2015).
- <sup>109</sup>F. Graffitti, V. D’Ambrosio, M. Proietti, J. Ho, B. Piccirillo, C. de Lisio, L. Marrucci, and A. Fedrizzi, “Hyperentanglement in structured quantum light,” *Phys. Rev. Res.* **2**, 043350 (2020).
- <sup>110</sup>P. W. Shor, “Scheme for reducing decoherence in quantum computer memory,” *Phys. Rev. A* **52**, R2493–R2496 (1995).
- <sup>111</sup>R. Bekenstein, I. Pikovski, H. Pichler, E. Shahmoon, S. F. Yelin, and M. D. Lukin, “Quantum metasurfaces with atom arrays,” *Nat. Phys.* **16**, 676–681 (2020).